Aalborg University

Masters Thesis

Terahertz Response of Semiconductor 2D-electron gas device

Written by:
Simon T. K. Schmidt

Supervised by:
Thomas M. Søndergaard

Department of Materials and Production

Fall semester 2019

3rd january 2020

AALBORG UNIVERSITY
STUDENT REPORT

Department of Materials and Production
Aalborg University
http://www.mp.aau.dk

Title:
Terahertz Response of Semiconductor 2D-electron gas device

Project period:
Fall semester 2019

Participant:
Simon Tankred Karkov Schmidt

Supervisor:
Thomas Møller Søndergaard

Number of pages: 37

Date of completion:
3rd january 2020

Abstract

This thesis will cover the creation of a model for terahertz response of a 2D semiconducting structure. The first part of the thesis contains the theoretical basis upon which the model will be built. After this the guided mode for a similar structure is calculated. Primarily to help in finding suitable initial conditions for the more advanced model. Following this a model based upon Green's functions is derived. Though the final model seem to produce usable results, the results should only be used as a guideline. It is not possible to increase the resolution of the discretisation to a point where it produces stable results due to memory usage.

The content of this report is freely available, but publication (with reference) may only be pursued due to agreement with the author.

Table of Contents

Preface

I would like to start by thank my supervisor Thomas Møller Søndergaard for all his help during the research for this thesis, and his helpful comments and suggestions for improvements.

All calculation for this thesis were performed in Matlab. All figures, graphs, and illustrations is my own work. Appended to this thesis is a zip-file containing the Matlab scripts used in calculating the terahertz response.

Simon Tankred Karkov Schmidt

1 Introduction

Until recently there were only a few sources of terahertz radiation[1]. With an increasing number of sources available researching possible applications becomes easier. Some application are explosives detection[2], communications [3], medical imagining [4] etc. The safety of therahertz radiation is also being researched [5, 6]

With all the research into therahertz and its effect we need theoretical model for how media responds to it. In this report I will attempt to create a model for the terahertz response of a semiconductor. This will be achieved by implementing Green's function for a scatterer placed on a layered semi-conduction structure. To achieve a expectation of how the material might behave, and to help set boundary conditions for the calculations, the guided modes of a similar structure will be explored.

Chapter 2 lays a theoretical basis for the calculations. It contains a short introduction to Maxwell's equations, a derivation of Fresnel reflection and transmission, and an overview of the used Green's function.

Chapter 3 describes how the guided modes is found, and presents the results.

Chapter 4 describes how the terahertz response is calculated, and presents the results.

In chapter 5 the result of the thesis will be evaluated.

2 Theory

This chapter will set a theoretical basis for calculation of the terahertz response. First there will be a short overwiev of the Maxwell equations. Secondly the Fresnel equations for reflection and transmission will be derived. Lastly greens function will be descrideb. Since the calculations of the terahertz respone is made for p-polarised light, s-polarised light is not included in this chapter. This chapter is based upon [7–9].

2.1 Maxwell equations

Starting with the differential form of Maxwell's equations

$$\nabla \times \mathbf{E}(\mathbf{r},t) = -\frac{\partial \mathbf{B}(\mathbf{r},t)}{\partial t}\,, \tag{2.1}$$

$$\nabla \cdot \mathbf{D}(\mathbf{r},t) = \rho(\mathbf{r},t)\,, \tag{2.2}$$

$$\nabla \times \mathbf{H}(\mathbf{r},t) = \mathbf{J}(\mathbf{r},t) + \frac{\partial \mathbf{D}(\mathbf{r},t)}{\partial t}\,, \tag{2.3}$$

$$\nabla \cdot \mathbf{B}(\mathbf{r},t) = 0\,, \tag{2.4}$$

where $\mathbf{E}$ is the electric field, $\mathbf{B}$ is the magnetic induction field, $\mathbf{D}$ is the electric displacement filed, ρ is the free charge density, $\mathbf{J}$ is the free current density, and $\mathbf{H}$ is the magnetic field, all at position $\mathbf{r}$ at time t.

In isotropic linear media

$$\mathbf{B}(\mathbf{r},t) = \mu_0(\mathbf{H}(\mathbf{r},t) + \mathbf{M}(\mathbf{r},t))\,, \tag{2.5}$$

$$\mathbf{D}(\mathbf{r},t) = \epsilon_0\mathbf{E}(\mathbf{r},t) + \mathbf{P}(\mathbf{r},t)\,, \tag{2.6}$$

where $\mathbf{M}(\mathbf{r},t)$ is the magnetisation, and $\mathbf{P}(\mathbf{r},t)$ is the polarisation density given by

$$\mathbf{P}(\mathbf{r},t) = \epsilon_0 \int_{-\infty}^{t} \chi_e(\mathbf{r},t-t')\mathbf{E}(\mathbf{r},t)\,\mathrm{d}t'\,, \tag{2.7}$$

$$\mathbf{M}(\mathbf{r},t) = \chi_m\mathbf{E}(\mathbf{r},t)\,, \tag{2.8}$$

where χ is the susceptibility of the media. In this thesis the magnetisation will be considered negligible, giving $\mathbf{B} = \mu_0\mathbf{H}$ The current density can be given as the sum of source currents $\mathbf{J}_s$, and current generated by the electric field (Ohms law).

$$\mathbf{J}(\mathbf{r},t) = \mathbf{J}_s(\mathbf{r},t) + \int_{-\infty}^{t} \sigma(\mathbf{r},t-t')\mathbf{E}(\mathbf{r},t)\,\mathrm{d}t'\,. \tag{2.9}$$

By Fourier Transform[10] it is possible to move from time domain t to frequency domain ω as

$$\mathbf{J}(\mathbf{r},t) = \frac{1}{\sqrt{2\pi}} \int_{-\infty}^{\infty} \mathbf{J}(\mathbf{r},\omega)\, \mathrm{e}^{-\mathrm{i}\omega t}\, \mathrm{d}\omega\,, \tag{2.10}$$

$$\mathbf{J}(\mathbf{r},\omega) = \frac{1}{\sqrt{2\pi}} \int_{-\infty}^{\infty} \mathbf{J}(\mathbf{r},t)\, \mathrm{e}^{\mathrm{i}\omega t}\, \mathrm{d}t\,. \tag{2.11}$$

A similar relation can be derive for $\mathbf{E}$, $\mathbf{B}$, $\mathbf{D}$, ρ, $\mathbf{H}$, $\mathbf{P}$, χ, and σ.

By the convolution theorem[10] the integrals eqs. (2.7) and (2.9) is simplified to products in the frequency domain to

$$\mathbf{P}(\mathbf{r},\omega) = \epsilon_0 \chi(\mathbf{r},\omega)\mathbf{E}(\mathbf{r},\omega)\,, \tag{2.12}$$

$$\mathbf{J}(\mathbf{r},\omega) = \mathbf{J}_s(\mathbf{r},\omega) + \sigma(\mathbf{r},\omega)\mathbf{E}(\mathbf{r},\omega) \tag{2.13}$$

Calculating the Fourier transform of eq. (2.3) gives

$$\nabla \times \mathbf{H}(\mathbf{r},\omega) = \mathbf{J}_s(\mathbf{r},\omega) + \sigma(\mathbf{r},\omega)\mathbf{E}(\mathbf{r},\omega) - \mathrm{i}\omega\epsilon_0(1+\chi(\mathbf{r},\omega))\mathbf{E}(\mathbf{r},\omega)\,. \tag{2.14}$$

Treating the induced currents as polarisation eq. (2.6) can be redefined to

$$\mathbf{D}(\mathbf{r},\omega) = \epsilon_0 \epsilon(\mathbf{r},\omega)\mathbf{E}(\mathbf{r},\omega)\,, \tag{2.15}$$

where

$$\epsilon(\mathbf{r},\omega) \equiv \left(1 + \chi(\mathbf{r},\omega) + \frac{\mathrm{i}\sigma(\mathbf{r},\omega)}{\omega\epsilon_0}\right). \tag{2.16}$$

With this it is possible to transform the differential Maxwell equations

$$\nabla \times \mathbf{E}(\mathbf{r},\omega) = \mathrm{i}\omega\mu_0\mathbf{H}(\mathbf{r},\omega)\,, \tag{2.17}$$

$$\nabla \cdot \mathbf{D}(\mathbf{r},\omega) = \rho(\mathbf{r},\omega)\,, \tag{2.18}$$

$$\nabla \times \mathbf{H}(\mathbf{r},\omega) = \mathbf{J}_s(\mathbf{r},\omega) - \mathrm{i}\omega\epsilon_0\epsilon(\mathbf{r},\omega)\mathbf{E}(\mathbf{r},\omega)\,, \tag{2.19}$$

$$\nabla \cdot \mathbf{B}(\mathbf{r},\omega) = 0\,, \tag{2.20}$$

From these equations it is possible to derive a set of equations for the electric field and the magnetic field that is only dependant itself and source current.

$$\nabla \times \nabla \times \mathbf{E}(\mathbf{r},\omega) - \omega^2\epsilon_0\mu_0\epsilon(\mathbf{r},\omega)\mathbf{E}(\mathbf{r},\omega) = \mathrm{i}\omega\mu_0\mathbf{J}_s(\mathbf{r},\omega)\,, \tag{2.21}$$

$$\frac{\mathrm{i}}{\omega\epsilon_0}\nabla \times \frac{1}{\epsilon(\mathbf{r},\omega)}\nabla \times \mathbf{H}(\mathbf{r},\omega) - \mathrm{i}\omega\mu_0\mathbf{H}(\mathbf{r},\omega) = \frac{-\mathrm{i}}{\omega\epsilon_0\epsilon(\mathbf{r},\omega)}\nabla \times \mathbf{J}_s(\mathbf{r},\omega)\,, \tag{2.22}$$

In a regions where the dielectric constant is independent of position and frequency ($\epsilon(\mathbf{r},\omega) = \epsilon$), and the source current density vanishes these become

$$(\nabla^2 + k_0^2\epsilon)\mathbf{E}(\mathbf{r},\omega) = \mathbf{0}\,, \qquad \nabla \cdot \mathbf{E}(\mathbf{r},\omega) = 0\,, \tag{2.23}$$

$$(\nabla^2 + k_0^2\epsilon)\mathbf{H}(\mathbf{r},\omega) = \mathbf{0}\,, \qquad \nabla \cdot \mathbf{H}(\mathbf{r},\omega) = 0\,, \tag{2.24}$$

Using the free-space wave-number $k_0 = \omega c^{-1}$, where $c^{-1} = \sqrt{\epsilon_0\mu_0}$.

2.1.1 Poynting Vector

The time averaged Poynting vector is defined as

$$\langle \mathbf{S} \rangle \equiv \frac{1}{2} |\mathbf{E} \times \mathbf{H}^*| \,. \tag{2.25}$$

It is the scattered magnetic field that will be calculated. Therefore a solution to eq. (2.25) that is only dependant of the magnetic field will be derived. Using eq. (2.19), assuming that the source current density vanishes and $\epsilon(\mathbf{r}, \omega) = \epsilon$ eq. (2.25) gives

$$\langle \mathbf{S} \rangle = \frac{1}{2} \left| \frac{\mathrm{i}}{\omega \epsilon_0 \epsilon} (\nabla \times \mathbf{H}) \times \mathbf{H}^* \right| . \tag{2.26}$$

The product $\nabla \times \mathbf{H}$ can be derived to

$$\nabla \times \mathbf{H} = \mathrm{i}\mathbf{k} \times \mathbf{H} \,, \tag{2.27}$$

where $\mathbf{k}$ is the wave-vector. Additionally the refractive index $n = ck\omega^{-1} = \sqrt{(\epsilon)}$, assuming that $mu = 1$ simplifying the Poynting vector to

$$\langle \mathbf{S} \rangle = \frac{1}{2c\epsilon_0 n} \left| \left(\hat{k} \times \mathbf{H} \right) \times \mathbf{H}^* \right| = \frac{\hat{k} |H|^2}{2c\epsilon_0 n} \,. \tag{2.28}$$

2.1.2 Cross Section

The scattering cross-section is defined as

$$\sigma_{\text{scat}} \equiv \frac{P_{\text{scat}}}{I_i} \,, \tag{2.29}$$

where P_{scat} is the total scattered power, and I_i is the power per unit area. I_i can be found as

$$I_i = \frac{|H_0|^2}{2c\epsilon_0 n_i} \,, \tag{2.30}$$

where n_i is the refractive index of the incident material. The total scattered power can be found from the Poynting vector as

$$P_{\text{scat}} = \int_\theta |\langle \mathbf{S}_{\text{scat}}(\mathbf{r}, \boldsymbol{\theta}) \rangle| r \, \mathrm{d}\theta \,. \tag{2.31}$$

2.2 Fresnel Reflection and Transmission

In this section the coefficients for reflection and transmission for p-polarised light will de derived. First the coefficients (r_{12}, t_{12}) will be derived for a single interface. $r_1 2, t_1 2$ will then be used to derive the coefficients (r_{1M}, t_{1M}), for a structue consisting of M layers.

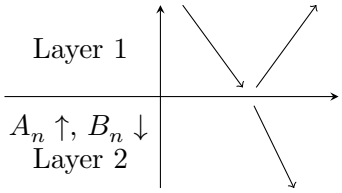

Figure 2.1: *Illustration of reflection and transmission at single interface.*

2.2.1 Single Interface

In fig. 2.1 the interface for which r_{12}, t_{12} will be derived is shown. This interface has the following boundary conditions:

$$H_1 = H_2\,, \tag{2.32}$$

$$\frac{1}{\epsilon_1}\frac{\partial H_1}{\partial y} = \frac{1}{\epsilon_2}\frac{\partial H_2}{\partial y}\,, \tag{2.33}$$

when $y = 0$. The magnetic field used is

$$H_n = \left(A_n\,\mathrm{e}^{-\mathrm{i}ky_y} + B_n\,\mathrm{e}^{\mathrm{i}ky_y}\right)f(x,\omega)\,, \tag{2.34}$$

where $f(x,\omega)$ is the time and x dependency of the field. This does not contribute to the coefficients, nor to the derivation, and will be neglected. The incident wave propagates downwards with amplitude B_1. The reflected wave propagates upwards with amplitude A_1. The transmitted wave propagates downwards with amplitude B_2. There is no wave associated with A_2, so $A_2 = 0$ With this the boundary conditions becomes

$$B_1 + A_1 = B_2\,, \tag{2.35}$$

$$\frac{k_{y1}}{\epsilon_1}(B_1 - A_1) = \frac{k_{y2}}{\epsilon_2}B_2\,. \tag{2.36}$$

The reflection coefficient is given as

$$r_{12} = \frac{A_1}{B_1}\,. \tag{2.37}$$

r_{12} can be calculated by isolating B_2 in the boundary conditions, setting them equal to each other, and isolating for r_{12}

$$B_1 + A_1 = \frac{k_{y1}\epsilon_2}{k_{y2}\epsilon_1}(B_1 - A_1)\,, \tag{2.38}$$

$$B_1\left(1 - \frac{k_{y1}\epsilon_2}{k_{y2}\epsilon_1}\right) = A_1\left(1 + \frac{k_{y1}\epsilon_2}{k_{y2}\epsilon 1}\right), \tag{2.39}$$

$$\frac{A_1}{B_1} = \frac{1 - \frac{k_{y1}\epsilon_2}{k_{y2}\epsilon_1}}{1 + \frac{k_{y1}\epsilon_2}{k_{y2}\epsilon 1}} = \frac{k_{y1}\epsilon_2 - k_{y2}\epsilon_1}{k_{y1}\epsilon_2 + k_{y2}\epsilon_1}\,. \tag{2.40}$$

The transmission coefficient is given as

$$t_{12} = \frac{B_2}{B_1}\,. \tag{2.41}$$

t_{12} can be calculated by isolating A_1 in the boundary conditions, setting them equal to each other, and isolating for t_{12}

$$B_2 - B_1 = B_1 - \frac{k_{y2}\epsilon_1}{k_{y1}\epsilon_2}B_2\,, \tag{2.42}$$

$$2B_1 = B_2\left(1 + \frac{k_{y2}\epsilon_1}{k_{y1}\epsilon_2}\right), \tag{2.43}$$

$$\frac{B_2}{B_1} = \frac{2}{1 + \frac{k_{y2}\epsilon_1}{k_{y1}\epsilon_2}} = \frac{2k_{y1}\epsilon_2}{k_{y1}\epsilon_2 + k_{y2}\epsilon_1}\,. \tag{2.44}$$

Similarly it is possible to derive expressions for r_{21}, and t_{21}

$$r_{12} = \frac{k_{y1}\epsilon_2 - k_{y2}\epsilon_1}{k_{y1}\epsilon_2 + k_{y2}\epsilon_1}\,, \tag{2.45}$$

$$r_{21} = \frac{k_{y2}\epsilon_1 - k_{y1}\epsilon_2}{k_{y1}\epsilon_2 + k_{y2}\epsilon_1}\,, \tag{2.46}$$

$$t_{12} = \frac{2k_{y1}\epsilon_2}{k_{y1}\epsilon_2 + k_{y2}\epsilon_1}\,, \tag{2.47}$$

$$t_{21} = \frac{2k_{y2}\epsilon_1}{k_{y1}\epsilon_2 + k_{y2}\epsilon_1}\,. \tag{2.48}$$

2.2.2 Multilayer stucture

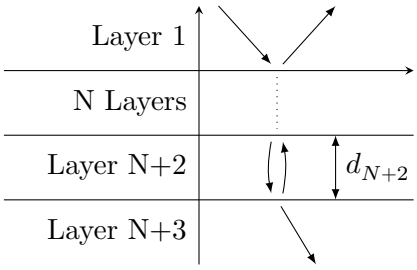

Figure 2.2: *Illustration of reflection and transmission for a multilayer structure.*

It is assumed that the reflection $r_{1,N+2}$, $r_{N+2,N+3}$ and transmission $t_{1,N+2}$, $t_{N+2,N+3}$ coefficients are known. Figure 2.2 illustrates the structure used to calculate $r_{1,N+3}$ and $t_{1,N+3}$. Between layers $N+1$ and $N+3$ the wave will oscillate transmitting a part each time it reaches an interface. Additionally there is a loss of $\mathrm{e}^{\mathrm{i}k_{y,N+2}d_{N+2}}$ travelling both up and down layer $N+2$. $r_{1,N+3}$ is calculated as

$$r_{1,N+3} = r_{1,N+1} + t_{1,N+1}r_{N+1,N+2}t_{N+1,1}\,\mathrm{e}^{2\,\mathrm{i}k_{y,N+2}d_{N+2}} + \tag{2.49}$$

$$t_{1,N+1} r_{N+1,N+2}^2 r_{N+1,1} t_{N+1,1} \, \mathrm{e}^{4\,\mathrm{i} k_{y,N+2} d_{N+2}} \ldots$$

$$= r_{1,N+2} + t_{1,N+2} t_{N+2,1} r_{N+2,N+3} \, \mathrm{e}^{2\,\mathrm{i} k_{y,N+2} d_{N+2}} \sum_{n=0}^{\infty} \left(r_{N+2,1} r_{N+2,N+3} \, \mathrm{e}^{2\,\mathrm{i} k_{y,N+2} d_{N+2}} \right)^n \tag{2.50}$$

$$= r_{1,N+2} + \frac{t_{1,N+2} t_{N+2,1} r_{N+2,N+3} \, \mathrm{e}^{2\,\mathrm{i} k_{y,N+2} d_{N+2}}}{1 - r_{N+2,1} r_{N+2,N+3} \, \mathrm{e}^{2\,\mathrm{i} k_{y,N+2} d_{N+2}}} \,. \tag{2.51}$$

The sum is solved by[11]

$$\sum_{n=0}^{inf} x^n = \frac{1}{1-x} \,, \quad -1 < x < 1 \,. \tag{2.52}$$

$t_{1,N+3}$ is calculated as

$$t_{1,N+3} = t_{1,N+2} t_{N+2,N+3} \, \mathrm{e}^{\mathrm{i} k_{y,N+2} d_{N+2}} + \tag{2.53}$$

$$t_{1,N+2} t_{N+2,N+3} r_{N+2,N+3} r_{N+2,1} \, \mathrm{e}^{3\,\mathrm{i} k_{y,N+2} d_{N+2}} \ldots$$

$$= t_{1,N+2} t_{N+2,N+3} \, \mathrm{e}^{\mathrm{i} k_{y,N+2} d_{N+2}} \sum_{n=0}^{\infty} \left(r_{N+2,N+3} r_{N+2,1} \, \mathrm{e}^{2\,\mathrm{i} k_{y,N+2} d_{N+2}} \right)^n \tag{2.54}$$

$$= \frac{t_{1,N+2} t_{N+2,N+3} \, \mathrm{e}^{\mathrm{i} k_{y,N+2} d_{N+2}}}{1 - r_{N+2,N+3} r_{N+2,1} \, \mathrm{e}^{2\,\mathrm{i} k_{y,N+2} d_{N+2}}} \,. \tag{2.55}$$

Similar derivations can be made for $r_{N+3,1}$ and $t_{N+3,1}$

$$r_{1,N+3} = r_{1,N+2} + \frac{t_{1,N+2} t_{N+2,1} r_{N+2,N+3} \, \mathrm{e}^{2\,\mathrm{i} k_{y,N+2} d_{N+2}}}{1 - r_{N+2,1} r_{N+2,N+3} \, \mathrm{e}^{2\,\mathrm{i} k_{y,N+2} d_{N+2}}} \,, \tag{2.56}$$

$$r_{N+3,1} = r_{N+3,N+2} + \frac{t_{1,N+2} t_{N+3,N+2} r_{N+3,N+2} \, \mathrm{e}^{2\,\mathrm{i} k_{y,N+2} d_{N+2}}}{1 - r_{N+2,1} r_{N+2,N+3} \, \mathrm{e}^{2\,\mathrm{i} k_{y,N+2} d_{N+2}}} \,, \tag{2.57}$$

$$t_{1,N+3} = \frac{t_{1,N+2} t_{N+2,N+3} \, \mathrm{e}^{\mathrm{i} k_{y,N+2} d_{N+2}}}{1 - r_{N+2,N+3} r_{N+2,1} \, \mathrm{e}^{2\,\mathrm{i} k_{y,N+2} d_{N+2}}} \,, \tag{2.58}$$

$$t_{N+3,1} = \frac{t_{N+3,N+2} t_{N+2,1} \, \mathrm{e}^{\mathrm{i} k_{y,N+2} d_{N+2}}}{1 - r_{N+2,N+3} r_{N+2,1} \, \mathrm{e}^{2\,\mathrm{i} k_{y,N+2} d_{N+2}}} \,. \tag{2.59}$$

The initial assumption of know $r_{1,N+2}$, $r_{N+2,N+3}$, $t_{1,N+2}$, and $t_{N+2,N+3}$ can be fulfilled by setting $N = 0$, where these coefficients are for a single interface. The found coefficients can then be used to calculate coefficients for $N = 1$ and so on.

2.3 Greens Function

In a layered structure Green's function may be split up into a direct part, and an indirect part. The direct part $g^{(d)}$ is identical to a structure consisting of one homogeneous material. The indirect part $g^{(i)}$ occurs as a result reflections from the layered structure.

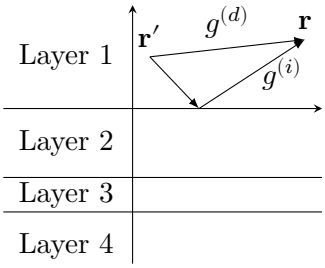

Figure 2.3: *Illustration of Green's function with contributions directly from the source and indirectly reflected on a layered structure.*

2.3.1 Direct Green's function

At any point the magnetic field must be a solution to eq. (2.24). Choosing a Green's function that satisfies

$$(\nabla^2 + k_0^2\epsilon_u)\mathbf{g}_u^{(d)}(\mathbf{r},\mathbf{r}') = -\delta(\mathbf{r},\mathbf{r}')\,, \tag{2.60}$$

the magnetic field at any point $\mathbf{r} \in \Omega_i$ can be found as

$$H(\mathbf{r}) = H_0(\mathbf{r}) - \oint_{C_1} \left(\mathbf{g}_1^{(d)}(\mathbf{r},\mathbf{r}')\hat{\mathbf{n}}'\cdot\nabla' H(\mathbf{r}') - H(\mathbf{r}')\hat{\mathbf{n}}'\cdot\nabla\mathbf{g}_1^{(d)}(\mathbf{r},\mathbf{r}')\right)\mathrm{d}l' \quad \mathbf{r}\in\Omega_1\,, \tag{2.61}$$

$$H(\mathbf{r}) = \oint_{C_s} \left(\mathbf{g}_s^{(d)}(\mathbf{r},\mathbf{r}')\hat{\mathbf{n}}'\cdot\nabla' H(\mathbf{r}') - H(\mathbf{r}')\hat{\mathbf{n}}'\cdot\nabla\mathbf{g}_s^{(d)}(\mathbf{r},\mathbf{r}')\right)\mathrm{d}l' \quad \mathbf{r}\in\Omega_s\,, \tag{2.62}$$

outside 1 the scatterer, and inside s the scatterer respectively. C_u is a curve following the surface on the scatter just outside 1, or inside s.

Green's function is chosen to be

$$g_u^{(d)} = \frac{\mathrm{i}}{4}H_0^{(1)}(k_0 n_u|\mathbf{r}-\mathbf{r}'|)\,, \tag{2.63}$$

where $H_0^(1)$ a zero'th order Hankel function of type 1.

2.3.2 Indirect Green's function

The sum of $g = g^(d) + g^(i)$ must satisfy

$$(\nabla^2 + k_0^2\epsilon_u)\mathbf{g}(\mathbf{r},\mathbf{r}') = -\delta(\mathbf{r},\mathbf{r}')\,, \tag{2.64}$$

The chosen direct Green's function does not satisfy boundary conditions at the interfaces between layers. To remedy this the indirect Green's function must be chosen such that the boundary conditions are satisfied. Expressing $g^(d)$ as plane waves

$$g^{(d)} = \frac{i}{2\pi}\int_0^\infty \frac{\cos(k_x|x-x'|\,\mathrm{e}^{\mathrm{i}k_{y,1}(y-y')})}{k_{y,1}}\,\mathrm{d}k_x\,, \tag{2.65}$$

where $k_{y,i} = \sqrt{k_0^2 n_i^2 - k_x^2}$, show that when $y > y'$ there are upwards propagating components, and when $y < y'$ there are downwards propagating components. The downward plane waves will be partially reflected, and transmitted. With this in mind it is possible to construct the indirect Green' function

$$g^{(i)}(\mathbf{r}, \mathbf{r}') = \frac{i}{2\pi} \int_0^\infty \frac{\cos(k_x|x - x'|r(k_x)\, \mathrm{e}^{\mathrm{i}k_{y,1}(y+y')})}{k_{y,1}} \, \mathrm{d}k_x \,, \tag{2.66}$$

for $\mathbf{r}$ above the interface between layers 1 and 2.

$$g^{(i)}(\mathbf{r}, \mathbf{r}') = \frac{i}{2\pi} \int_0^\infty \frac{\cos(k_x|x - x'|t(k_x)\, \mathrm{e}^{\mathrm{i}k_{y,1}y'}\, \mathrm{e}^{\mathrm{i}k_{y,1} - ik_{y,4}(y+d)})}{k_{y,1}} \, \mathrm{d}k_x \,, \tag{2.67}$$

for $\mathbf{r}$ below the interface between layers 3 and 4. $r(k_x)$, $t(k_x)$ is the Fresnel reflection coefficient described in section 2.2. d is the total thickness of layers 2 and 3. It is not possible to solve these integrals analytically, they must therefore be solved numerically. This is complicated by the reflection coefficient

$$r_{12} = \frac{k_{y1}\epsilon_2 - k_{y2}\epsilon_1}{k_{y1}\epsilon_2 + k_{y2}\epsilon_1} \approx \frac{\epsilon_2 - \epsilon_1}{\epsilon_2 + \epsilon_1} + \frac{k_0^2 \epsilon_1 \epsilon_2 (\epsilon_2 - \epsilon_1)}{k x^2 (\epsilon_2 + \epsilon_1)^2} \,, \tag{2.68}$$

approaching a constant value as k_x increases. Though with $g^{(i)}$ can be approximated to

$$g^{(i)}(\mathbf{r}, \mathbf{r}') \approx \frac{\epsilon_2 - \epsilon_1}{\epsilon_2 + \epsilon_1} \frac{i}{2\pi} \int_0^\infty \frac{\cos(k_x|x - x'|\, \mathrm{e}^{\mathrm{i}k_{y,1}(y+y')})}{k_{y,1}} \, \mathrm{d}k_x \,, \tag{2.69}$$

as $x - x' \to 0$ and $y + y' \to 0$. This is similar to eq. (2.65) giving

$$g^{(i)}(\mathbf{r}, \mathbf{r}') \approx \frac{\epsilon_2 - \epsilon_1}{\epsilon_2 + \epsilon_1} \frac{\mathrm{i}}{4} H_0^{(1)}(k_0 n_1 |\tilde{\mathbf{r}} - \mathbf{r}'|) \,, \tag{2.70}$$

where $\tilde{\mathbf{r}} = \mathbf{r} \cdot (\hat{x} - \hat{y})$ is the mirror point of $\mathbf{r}$. Inserting this approximation into eq. (2.66)

$$\begin{aligned} g^{(i)}(\mathbf{r}, \mathbf{r}') = {} & \frac{\epsilon_2 - \epsilon_1}{\epsilon_2 + \epsilon_1} \frac{\mathrm{i}}{4} H_0^{(1)}(k_0 n_1 |\tilde{\mathbf{r}} - \mathbf{r}'|) + \\ & \frac{i}{2\pi} \int_0^\infty \frac{\cos(k_x|x - x'|\left(r(k_x) - \frac{\epsilon_2 - \epsilon_1}{\epsilon_2 + \epsilon_1}\right) \mathrm{e}^{\mathrm{i}k_{y,1}(y+y')})}{k_{y,1}} \, \mathrm{d}k_x \end{aligned} \tag{2.71}$$

In this integral the integrand goes toward zero, as k_x increases making it easier to solve numerically. There are two sources for potential poles when solving this integral. First there is $k_{y,1}$ secondly there is the reflection coefficient. These poles can be avoided by integrating parts of the integral in for complex k_x.

2.3.3 Field Near Scatterer

This section will focus on calculating the field on both sides of the scatterer surface. For convenience the following notation is introduced

$$\phi(\mathbf{r}) \equiv \hat{\mathbf{n}} \cdot \nabla H_u(\mathbf{r}) \tag{2.72}$$

as the normal derivative of the field.

The surface of the scatterer is partitioned into N segments. It is assumed that the field is constant within each segment. Using $\mathbf{p}(t)$, where t is the distance travelled along the scatterer surface, as the position on the scatterer, the magnetic field and its derivative can be approximated as

$$H_u(\mathbf{p}(t)) \approx \sum_{i=1}^{N} H_{u,i} f_i(t)\,, \tag{2.73}$$

$$\phi_u(\mathbf{p}(t)) \approx \sum_{i=1}^{N} \phi_u u, i f_i(t)\,, \tag{2.74}$$

where

$$f_i(t) = \begin{cases} 1, t_{\text{start},i} < t < t_{\text{end},i} \\ 0, \text{otherwise} \end{cases}\,. \tag{2.75}$$

Inserting these into eqs. (2.61) and (2.62), with point matching applied results in

$$H_{1,i} = H_{0,1} - \sum_{j=1}^{N} \left(A_{ij}^{(1)} \phi 1, j - B_{ij}^{(1)} H1, j \right), \tag{2.76}$$

$$H_{2,i} = \sum_{j=1}^{N} \left(A_{ij}^{(2)} \phi 2, j - B_{ij}^{(2)} H2, j \right), \tag{2.77}$$

where $H_{0,i} = H_0(\mathbf{s}_i)$, and

$$A_{ij}^{(u)} = \lim_{\mathbf{r}\to\mathbf{s}} \int g_u(\mathbf{r}, \mathbf{s}(t)) f_j(t)\, \mathrm{d}t\,, \tag{2.78}$$

$$B_{ij}^{(u)} = \lim_{\mathbf{r}\to\mathbf{s}} \int (\hat{\mathbf{n}}' \cdot \nabla' g_u(\mathbf{r}, \mathbf{s}(t))) f_j(t)\, \mathrm{d}t\,. \tag{2.79}$$

are elements in matrices $\overline{\overline{A}}^{(u)}$ and $\overline{\overline{B}}^{(u)}$. Defining

$$\overline{H}_u \equiv [H_{u,1}; H_{u,2}; \cdots H_{u,N}]\,, \tag{2.80}$$

$$\overline{\phi}_u \equiv [\phi_{u,1}; \phi_{u,2}; \cdots \phi_{u,N}]\,, \tag{2.81}$$

as column-vector describing H and ϕ at the segment positions on the scatterer. Using these it is possible to reform eqs. (2.76) and (2.77) into matrix form

$$\left(\overline{\overline{I}} - \overline{\overline{B}}^{(1)} \right) \overline{H}_1 + \overline{\overline{A}}^{(1)} \overline{\phi}_1 = \overline{H}_0\,, \tag{2.82}$$

$$\left(\overline{\overline{I}} + \overline{\overline{B}}^{(s)}\right)\overline{H}_s + \overline{\overline{A}}^{(s)}\overline{\phi}_s = \overline{0}\,. \tag{2.83}$$

By the boundary conditions

$$\begin{aligned}\overline{H}_1 &= \overline{H}_s\,,\\ \epsilon_1^{-1}\overline{\phi}_1 &= \epsilon_s^{-1}\overline{\phi}_s\,,\end{aligned}$$

it is possible to formulate the matrix equation

$$\begin{bmatrix}\left(\overline{\overline{I}} - \overline{\overline{B}}^{(1)}\right) & \overline{\overline{A}}^{(1)}\\ \left(\overline{\overline{I}} + \overline{\overline{B}}^{(s)}\right) & -\frac{\epsilon_s}{\epsilon_1}\overline{\overline{A}}^{(s)}\end{bmatrix}\begin{bmatrix}\overline{H}\\ \overline{\phi}_1\end{bmatrix} = \begin{bmatrix}\overline{H}_0\\ \overline{0}\end{bmatrix}. \tag{2.84}$$

Solving this equation for $\overline{H}$ and $\overline{\phi}$ makes it possible to calculate the field at any point with eqs. (2.61) and (2.62).

3 Guided Mode

This chapter focuses on calculation of Guided mods in a 2-dimensional structure. It is intended to give an approximate idea of how the terahertz response changes when changing the structure, as well as guiding the choice of initial conditions for the slower calculations using Green's function.

3.1 Calculation

In a four layer structure as illustrated in fig. 3.1 the magnitude of the magnetic field can be expressed as

$$H_n(x,y,t) = (A_n\,\mathrm{e}^{ik_y(y-y_n)} + B_n\,\mathrm{e}^{-ik_y(y-y_n)})\,\mathrm{e}^{-ik_x x}\,\mathrm{e}^{i\omega t} \tag{3.1}$$

For layer one and two $y_n = 0$, for layer three $y_3 = -d_2$, for layer four $y_4 = -(d_2 + d_3)$,

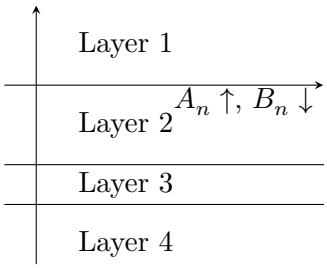

Figure 3.1: *Structure used in calculation of guided modes..*

where d_n is the thickens of layer n

At the interface between two layers n and $n+1$ the field is continuous so

$$H_n = H_{n+1} \tag{3.2}$$

$$\frac{1}{\epsilon_n}\frac{\partial H_n}{\partial y} = \frac{1}{\epsilon_{n+1}}\frac{\partial H_{n+1}}{\partial y}\,. \tag{3.3}$$

In an isolated system $B_1 = 0$ and $A_4 = 0$ Using A_1 as a fixed values it is possible to calculate the other coefficients as

$$A_2 = \frac{A_1}{2}(1+\kappa_{21}) \tag{3.4}$$

$$B_2 = \frac{A_1}{2}(1-\kappa_{21}) \tag{3.5}$$

$$A_3 = \frac{A_2}{2} e^{-ik_{y2}d_2}(1+\kappa_{32}) + \frac{B_2}{2} e^{ik_{y2}d_2}(1-\kappa_{32}) \tag{3.6}$$

$$B_3 = \frac{A_2}{2} e^{-ik_{y2}d_2}(1-\kappa_{32}) + \frac{B_2}{2} e^{ik_{y2}d_2}(1+\kappa_{32}) \tag{3.7}$$

$$B_4 = A_3 e^{-ik_y 3d_3} + B_3 e^{ik_y 3d_3}\,, \tag{3.8}$$

the constants used is defined as

$$\kappa_{mn} := \frac{\epsilon_M k_{yn}}{\epsilon_N k_{ym}} \tag{3.9}$$

$$k_{yn} := \sqrt{k_0^2 \epsilon_n - k_x^2}\,. \tag{3.10}$$

The guided modes is found by calculating

$$\begin{aligned} f(k_x) = {} & e^{-ik_{y2}d_2} e^{-ik_{y3}d_3}(1+\kappa_{21})(1+\kappa_{32})(1+\kappa_{43}) + \\ & e^{ik_{y2}d_2} e^{-ik_{y3}d_3}(1-\kappa_{21})(1-\kappa_{32})(1+\kappa_{43}) + \\ & e^{-ik_{y2}d_2} e^{ik_{y3}d_3}(1+\kappa_{21})(1-\kappa_{32})(1-\kappa_{43}) + \\ & e^{ik_{y2}d_2} e^{ik_{y3}d_3}(1-\kappa_{21})(1+\kappa_{32})(1-\kappa_{43})\,, \end{aligned} \tag{3.11}$$

for values of k_x and finding solutions to $f(k_x) = 0$.

$f(k_x)$ is calculated for 1001 values along each of the real and imaginary axis. The values are chosen on a logarithmic scale in the ranges:

$$\begin{aligned} 1.00001k_0 \leq \mathrm{Re}(k_x) \leq 2500k_0 \\ 0.00001k_0 \leq \mathrm{Im}(k_x) \leq 250k_0\,. \end{aligned}$$

The calculated matrix containing results is then evaluated to find potential for $f(k_x) = 0$. Where this is possible another matrix of values is calculated with this smaller range. The found value of k_x is then further refined with the Newton–Raphson method.

3.2 Found Modes

3.2.1 Dielectric Constant

Solving eq. (3.11) for zero values requires the dielectric constant of each layer. For layers one, two, and four a constant dielectric constant is used. A Drude model[12] is used to calculate the dielectric constant for layer three.

$$\sigma = \frac{e^2 N \tau}{m^*(1 - i\omega\tau)} \tag{3.12}$$

$$\epsilon = \epsilon_r + \frac{i\sigma}{\epsilon_0 \omega d}\,, \tag{3.13}$$

where N is the density of electrons, m^* is the effective mass, τ is the mean free time, ϵ_r is the high frequency dielectric constant, and d is the thickness. The electron density

and the thickness is variable, the rest are the constants $m^* = 0.2m_e$, $\epsilon_{\text{GaN}} = 5.35$, and $\tau = 1.14 \times 10^{-12}$ s. Figures 3.2 and 3.3 show the calculated dielectric constant. For each figure the calcluations is performed over a range of either wavelength, thickness, or electron density, with the other values chosen as *lambda* $= 3 \times 10^5$ nm, $d = 8$ nm, and $N = 7.5 \times 10^{12}$ cm^{-2}.

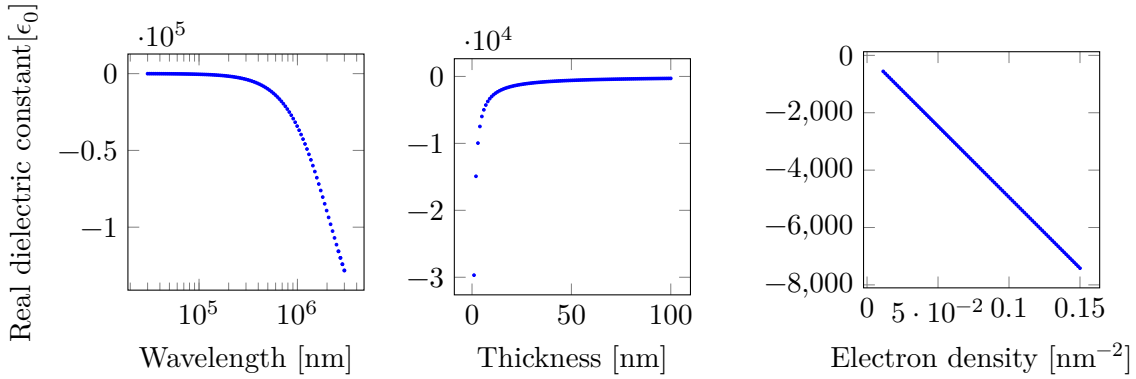

(a) *Varied wavelength, ranging from* 3×10^4 nm *to* 3×10^6 nm.

(b) *Varied thickness, ranging from* 1 nm *to* 100 nm.

(c) *Varied density of electrons, ranging from* 1×10^{12} cm^{-2} *to* 15×10^{12} cm^{-2}.

Figure 3.2: *Real dielectric constant of a thin layer of GaN carrying a current. The dielectric constant is calculated using a Drude model [12] Unless otherwise noted the wavelength is* 3×10^5 nm*, the layer is* 8 nm *thick, and the electron density is* 7.5×10^{12} cm^{-2}.

In figs. 3.2a and 3.3a ϵ is calculated over a range of wavelengths from 3×10^4 nm to 3×10^6 nm (10 THz to 0.1 THz), figs. 3.2b and 3.3b is calculated for thickness from 1 nm to 100 nm, and figs. 3.2c and 3.3c is calculaer for electron densities from 1×10^{12} cm^{-2} to 15×10^{12} cm^{-2}.

The material becomes increasingly metal like with increased electron density. A thin layer is also metal like, though it quickly becomes like a semi conductor. Increasing the wavelength also results in an increased real and imaginary part magnitude of the dielectric constant. Though unlike with electron density and thickness, the magnitude of the imaginary part increases faster than the real part.

3.2.2 Air in Layer One

The calculated dielectric constant can be used to find solutions to $f(k_x) = 0$ (eq. (3.11)), as described in section 3.1. In this section modes will be found for a structure where layer one is air, where $\epsilon_1 = 1$, layer two is AlGaN, where $\epsilon_2 = 5$, layer three is the doped layer of GaN with ϵ_3 calculated in section 3.2.1, and layer four is neutral GaN, with $\epsilon_4 = 5.35$.

Figures 3.4 to 3.11 shows the found modes. The modes is found over a range of either wavelength (3×10^4 nm to 3×10^6 nm), thickness of layer two (1 nm to 1000 nm), layer three (1 nm to 100 nm), or electron density (1×10^{12} cm^{-2} to 15×10^{12} cm^{-2}). A "standard" value is used for the other coefficients. These are $\lambda = 3 \times 10^5$ nm, $d_2 = 10$ nm,

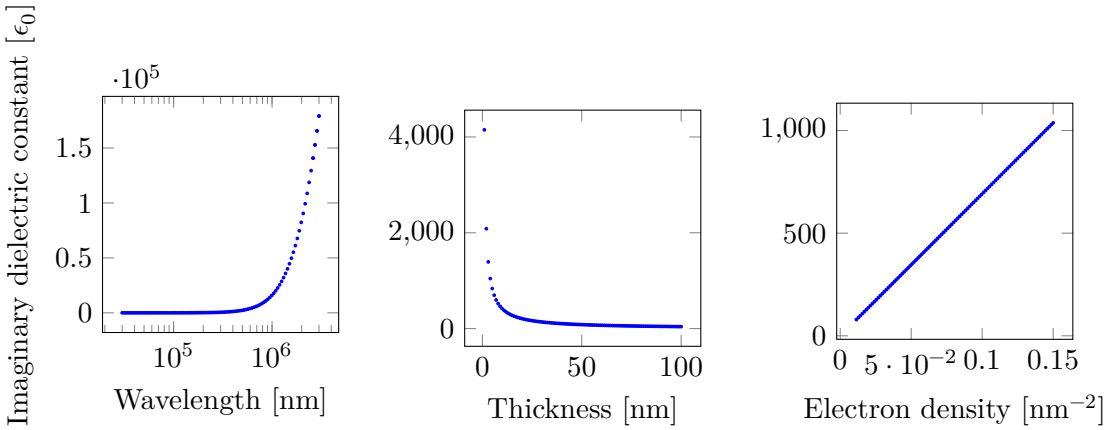

(a) *Varied wavelength, ranging from* 3×10^4 nm *to* 3×10^6 nm.

(b) *Varied thickness, ranging from* 1 nm *to* 100 nm.

(c) *Varied density of electrons, ranging from* 1×10^{12} cm^{-2} *to* 15×10^{12} cm^{-2}.

Figure 3.3: *Imaginary dielectric constant of a thin layer of GaN carrying a current. The dielectric constant is calculated using a Drude model [12] Unless otherwise noted the wavelength is* 3×10^5 nm*, the layer is* 8 nm *thick, and the electron density is* 7.5×10^{12} cm^{-2}.

$d_3 = 8$ nm, and $N = 7.5 \times 10^{12}$ cm^{-2}. For each range the modes is additionally calculated for three different values of either λ (6×10^4 nm, 3×10^5 nm, and 6×10^5 nm), d_2 (4 nm, 10 nm, and 25 nm, d_3 (2 nm, 8 nm, and 32 nm), and N (3.75×10^{12} cm^{-2}, 7.5×10^{12} cm^{-2}, and 1.125×10^{13} cm^{-2})

As shown in figs. 3.4 and 3.5 long wavelength results in two possible modes are found, though for the secondary modes, the real part of the modes is lower than the dielectric constants of the surrounding material, making these mode unusable for guided modes. The imaginary parts of the found modes is much lower than real parts, resulting in a potentially low loss. It is worth noting that short wavelengths results in the highest real mode, and is for most of the calculations. The only part where changing on of the other parameters results in a significant change in mode. The only deviation from this is the imaginary part with different electron densities, which is to be expected, since increasing N results in a more metal like structure, which in turn is expected to result in a lower loss.

Figures 3.6 and 3.7 illustrates that for the most part a change in thickness of layer two only results in a small variation in mode. The change is most prominent for low wavelength and a thin layer, or for low electron densities. It is also evident that the thickness of layer three only has a minor impact on the mode when compared to the thickness of layer two.

In figs. 3.8 and 3.9 it can be seen that the only secondary parameter radically influenced by the thickness oflayer three is wavelenegth. There is a drastic increase in the mode for a short wavelength (6×10^4 nm) when the thickness of layer three is increased. This is most prominent in the imaginary value. The figures also show that for other than low

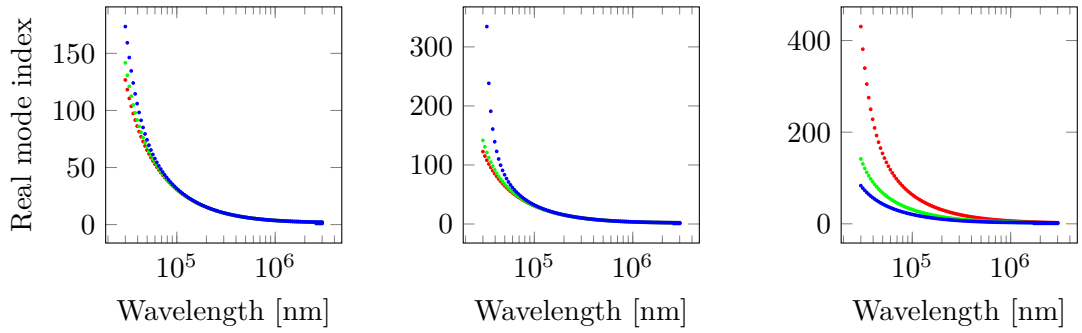

(a) *Varied thickness of layer two. Red*=4 nm, *Green*=10 nm, *Blue*=25 nm.

(b) *Varied thickness of layer three. Red*=2 nm, *Green*=8 nm, *Blue*=32 nm.

(c) *Varied density of electrons in layer three. Red*=3.75×10^{12} cm^{-2}, *Green*=7.5×10^{12} cm^{-2}, *Blue*=1.125×10^{13} cm^{-2}.

Figure 3.4: *Real mode of a four layer structure as illustrated in fig. 3.1. The modes is calculated with varying wavelengths over a logarithmic scale from* 3×10^4 nm *to* 3×10^6 nm *(*10 THz *to* 0.1 THz*). Layer one is air, layer two is AlGaN, layer three is GaN with additional free electrons, and layer four is neutral GaN. Unless otherwise noted the thickness of layer two is* 10 nm*, layer three is* 8 nm *thick, and the electron density of layer three is* 7.5×10^{12} cm^{-2}.

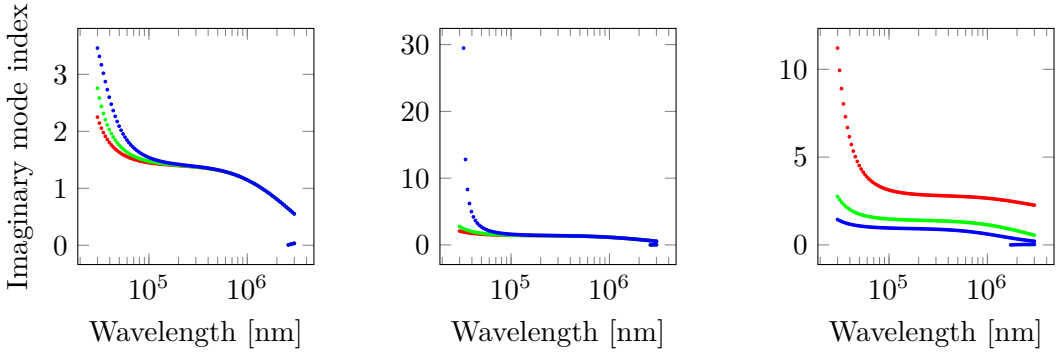

(a) *Varied thickness of layer two. Red*=4 nm, *Green*=10 nm, *Blue*=25 nm.

(b) *Varied thickness of layer three. Red*=2 nm, *Green*=8 nm, *Blue*=32 nm.

(c) *Varied density of electrons in layer three. Red*=3.75×10^{12} cm^{-2}, *Green*=7.5×10^{12} cm^{-2}, *Blue*=1.125×10^{13} cm^{-2}.

Figure 3.5: *Imaginary mode of a four layer structure as illustrated in fig. 3.1. The modes is calculated with varying wavelengths over a logarithmic scale from* 3×10^4 nm *to* 3×10^6 nm *(*10 THz *to* 0.1 THz*). Layer one is air, layer two is AlGaN, layer three is GaN with additional free electrons, and layer four is neutral GaN. Unless otherwise noted the thickness of layer two is* 10 nm*, layer three is* 8 nm *thick, and the electron density of layer three is* 7.5×10^{12} cm^{-2}.

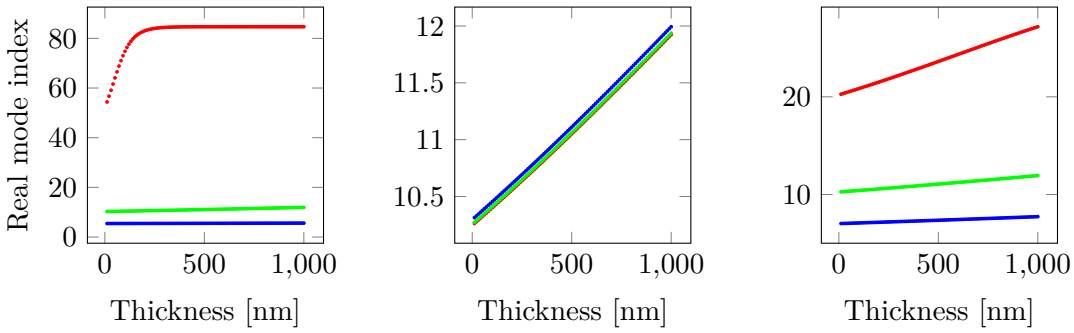

(a) *Varied wavelength. Red*=6×10^4 nm, *Green*=3×10^5 nm, *Blue*=6×10^5 nm.

(b) *Varied thickness of layer three. Red*=2 nm, *Green*=8 nm, *Blue*=32 nm.

(c) *Varied density of electrons in layer three. Red*=3.75×10^{12} cm^{-2}, *Green*=7.5×10^{12} cm^{-2}, *Blue*=1.125×10^{13} cm^{-2}.

Figure 3.6: *Real mode of a four layer structure as illustrated in fig. 3.1. The modes is calculated with varying thickness of layer two from* 1 nm *to* 1000 nm. *Layer one is air, layer two is AlGaN, layer three is GaN with additional free electrons, and layer four is neutral GaN. Unless otherwise noted the wavelength is* 3×10^5 nm *and layer three is* 8 nm *thick, and the electron density of layer three is* 7.5×10^{12} cm^{-2}.

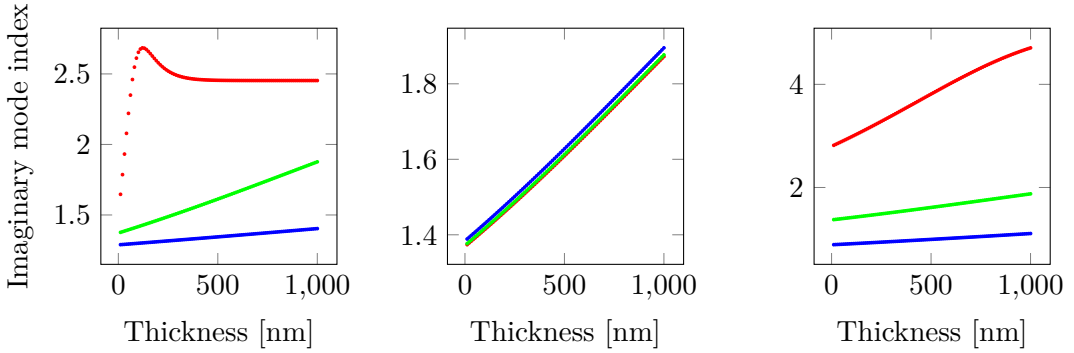

(a) *Varied wavelength. Red*=6×10^4 nm, *Green*=3×10^5 nm, *Blue*=6×10^5 nm.

(b) *Varied thickness of layer three. Red*=2 nm, *Green*=8 nm, *Blue*=32 nm.

(c) *Varied density of electrons in layer three. Red*=3.75×10^{12} cm^{-2}, *Green*=7.5×10^{12} cm^{-2}, *Blue*=1.125×10^{13} cm^{-2}.

Figure 3.7: *Imaginary mode of a four layer structure as illustrated in fig. 3.1. The modes is calculated with varying thickness of layer two from* 1 nm *to* 1000 nm. *Layer one is air, layer two is AlGaN, layer three is GaN with additional free electrons, and layer four is neutral GaN. Unless otherwise noted the wavelength is* 3×10^5 nm, *layer three is* 8 nm *thick, and the electron density of layer three is* 7.5×10^{12} cm^{-2}.

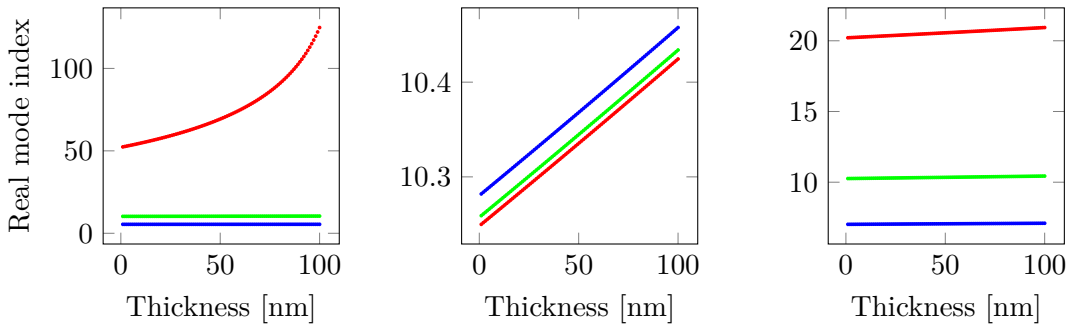

(a) *Varied wavelength.* *Red*=6×10^4 nm, *Green*=3×10^5 nm, *Blue*=6×10^5 nm.

(b) *Varied thickness of layer two.* *Red*=4 nm, *Green*=10 nm, *Blue*=25 nm.

(c) *Varied density of electrons in layer three.* *Red*=3.75×10^{12} cm^{-2}, *Green*=7.5×10^{12} cm^{-2}, *Blue*=1.125×10^{13} cm^{-2}.

Figure 3.8: *Real mode of a four layer structure as illustrated in fig. 3.1. The modes is calculated with varying thickness of layer three from* 1 nm *to* 100 nm*. Layer one is air, layer two is AlGaN, layer three is GaN with additional free electrons, and layer four is neutral GaN. Unless otherwise noted the wavelength is* 3×10^5 nm*, layer two is* 10 nm *thick, and the electron density of layer three is* 7.5×10^{12} cm^{-2}.

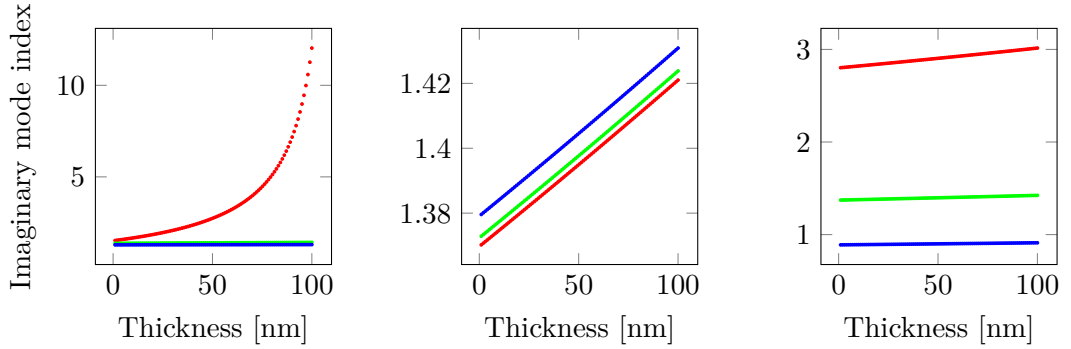

(a) *Varied wavelength.* *Red*=6×10^4 nm, *Green*=3×10^5 nm, *Blue*=6×10^5 nm.

(b) *Varied thickness of layer two.* *Red*=4 nm, *Green*=10 nm, *Blue*=25 nm.

(c) *Varied density of electrons in layer three.* *Red*=3.75×10^{12} cm^{-2}, *Green*=7.5×10^{12} cm^{-2}, *Blue*=1.125×10^{13} cm^{-2}.

Figure 3.9: *Imaginary mode of a four layer structure as illustrated in fig. 3.1. The modes is calculated with varying thickness of layer three from* 1 nm *to* 100 nm*. Layer one is air, layer two is AlGaN, layer three is GaN with additional free electrons, and layer four is neutral GaN. Unless otherwise noted the wavelength is* 3×10^5 nm*, layer two is* 10 nm *thick, and the electron density of layer three is* 7.5×10^{12} cm^{-2}.

wavelengths, that increasing the thickness of layer two only results in a minor increase in the mode

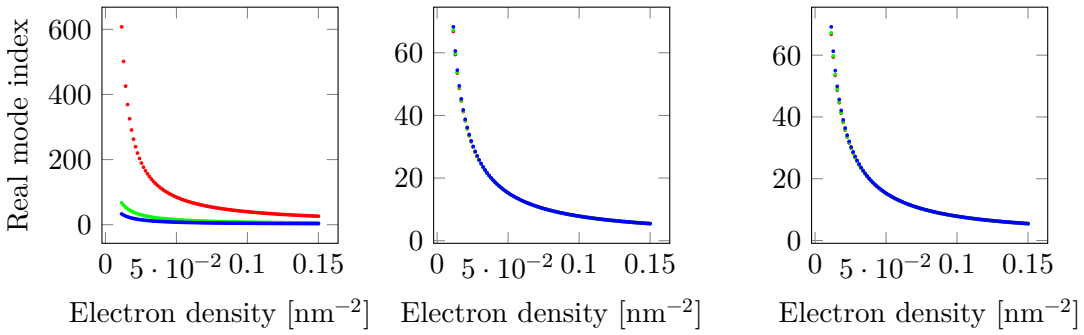

(a) *Varied wavelength. Red*=6×10^4 nm, *Green*=3×10^5 nm, *Blue*=6×10^5 nm.

(b) *Varied thickness of layer two. Red*=4 nm, *Green*=10 nm, *Blue*=25 nm.

(c) *Varied thickness of layer three. Red*=2 nm, *Green*=8 nm, *Blue*=32 nm.

Figure 3.10: *Real mode of a four layer structure as illustrated in fig. 3.1. The modes is calculated with varying electron densities in layer three from* 1×10^{12} cm^{-2} *to* 15×10^{12} cm^{-2}. *Layer one is air, layer two is AlGaN, layer three is GaN with additional free electrons, and layer four is neutral GaN. Unless otherwise noted the wavelength is* 3×10^5 nm, *layer two is* 10 nm *thick, and layer three is* 8 nm *thick.*

Figures 3.10 and 3.11 illustrates a clear connection between the electron density and the mode. They also show that the structure is most sensetive for wavelengths at low electron denseties. It is also clear that changing the thickness of either layer two or three only has a small effect on the mode.

In summary The thickness of each layer only seem to make a minor contribution to the possible modes. Though it is preferable that layer two is relatively thin to reduce the loss at low wavelengths. It is possible to tune the resonance frequency of the structure by varying the electron density. This coupled with the fact that a change in wavelength results in a change of mode, indicates that it is possible to create a structure that is sensitive to specific wavelengths.

3.2.3 Perfect Conductor as Layer One

This sections covers a caculation for a structure simmilar to the one described in section 3.2.2. The difference is that in this section layer one is a perfect conductor with $\epsilon_1 = -\infty$

Figures 3.12 to 3.19 shows the result of the calculation under the same constraints as in section 3.2.2.

As shown in figs. 3.12 and 3.13 the mode is depentant on the wavelength. The real part is nearly linear and flat in the range of wavelengths from 1×10^5 nm to 1×10^6 nm, with an seemingly exponential increase outside this range. Whereas the imaginary part for the most part exhibit an exponential increase with wavelength, nearing the real value

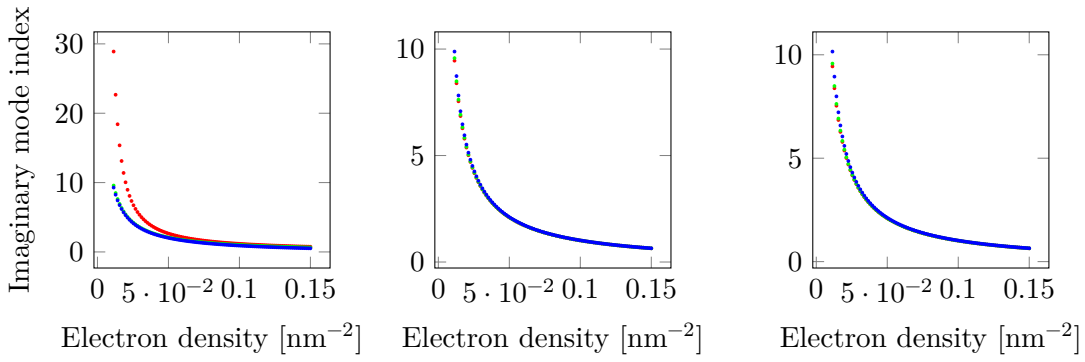

(a) *Varied wavelength. Red*=6×10^4 nm, *Green*=3×10^5 nm, *Blue*=6×10^5 nm.

(b) *Varied thickness of layer two. Red*=4 nm, *Green*=10 nm, *Blue*=25 nm.

(c) *Varied thickness of layer three. Red*=2 nm, *Green*=8 nm, *Blue*=32 nm.

Figure 3.11: *Imaginary mode of a four layer structure as illustrated in fig. 3.1. The modes is calculated with varying electron densities in layer three from* 1×10^{12} cm^{-2} *to* 15×10^{12} cm^{-2}*. Layer one is air, layer two is AlGaN, layer three is GaN with additional free electrons, and layer four is neutral GaN. Unless otherwise noted the wavelength is* 3×10^5 nm*, layer two is* 10 nm *thick, and layer three is* 8 nm *thick.*

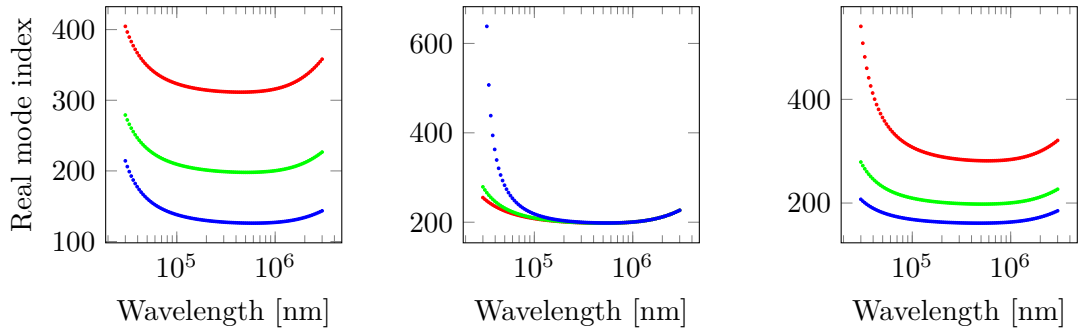

(a) *Varied thickness of layer two. Red*=4 nm, *Green*=10 nm, *Blue*=25 nm.

(b) *Varied thickness of layer three. Red*=2 nm, *Green*=8 nm, *Blue*=32 nm.

(c) *Varied density of electrons in layer three. Red*=3.75×10^{12} cm^{-2}, *Green*=7.5×10^{12} cm^{-2}, *Blue*=1.125×10^{13} cm^{-2}.

Figure 3.12: *Real mode of a four layer structure as illustrated in fig. 3.1. The modes is calculated with varying wavelengths over a logarithmic scale from* 3×10^4 nm *to* 3×10^6 nm *(*10 THz *to* 0.1 THz*). Layer one is a perfect conductor, layer two is AlGaN, layer three is GaN with additional free electrons, and layer four is neutral GaN. Unless otherwise noted the thickness of layer two is* 10 nm*, layer three is* 8 nm *thick, and the electron density of layer three is* 7.5×10^{12} cm^{-2}.

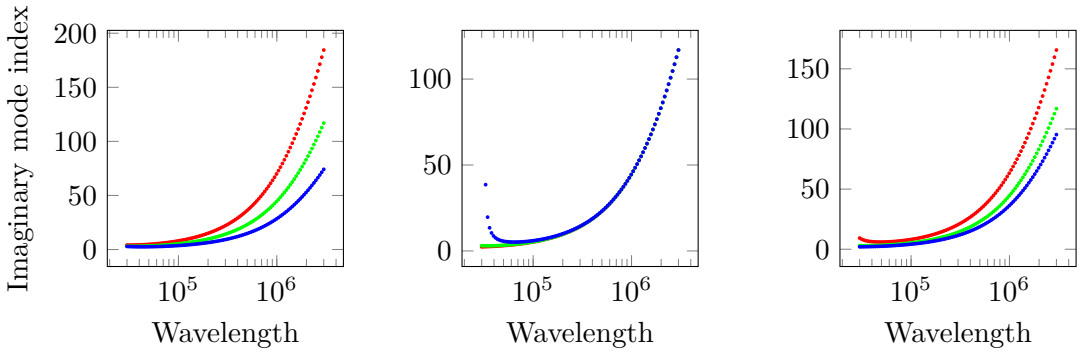

(a) *Varied thickness of layer two. Red*=4 nm, *Green*=10 nm, *Blue*=25 nm.

(b) *Varied thickness of layer three. Red*=2 nm, *Green*=8 nm, *Blue*=32 nm.

(c) *Varied density of electrons in layer three. Red*=$3.75 \times 10^{12}\,\mathrm{cm}^{-2}$, *Green*=$7.5 \times 10^{12}\,\mathrm{cm}^{-2}$, *Blue*=$1.125 \times 10^{13}\,\mathrm{cm}^{-2}$.

Figure 3.13: *Imaginary mode of a four layer structure as illustrated in fig. 3.1. The modes is calculated with varying wavelengths over a logarithmic scale from* 3×10^4 nm *to* 3×10^6 nm (10 THz *to* 0.1 THz). *Layer one is a perfect conductor, layer two is AlGaN, layer three is GaN with additional free electrons, and layer four is neutral GaN. Unless otherwise noted the thickness of layer two is* 10 nm, *layer three is* 8 nm *thick, and the electron density of layer three is* $7.5 \times 10^{12}\,\mathrm{cm}^{-2}$.

for high wavelengths. For a low electron density, or a thick third layer, which incidently also lowers the electron density, the imaginary part of the mode also seem to increase.

Figures 3.14 and 3.15 Show that increasing the thicknees of layer two results in a decreased mode, both real and imaginary. There is one exception, when the wavelength is low, the real part becomes constant when the layer becomes thicker, and the imaginary part show a slight increase, before leveling off. This indicates that the magnetic wave is contained within layer two.

From figs. 3.16 and 3.17 it can be derived that the thickness of layer three only has a small influence over the mode. There is one notable exception, this is when the wavelength is low (6×10^4 nm). Here both the real and imaginary mode increases with thickness, but most notably, for a thick layer two modes is found. In this mode the imaginary part dominates, resulting in a high loss. Which makes this mode unusable for a detector based on resonance.

Figures 3.18 and 3.19 show a clear correlation between the electron density and mode, regardless of the other parameters. As the electron density increases, the mode becomes lower.

3.2.4 Magnetic Field

In figs. 3.20 and 3.21 the magnetic field is plotted for a structure with air as the first layer. The mode used in the calcualtions is $n_m = 1.027\,116 \times 10^1 + 1.376\,384i$.

In figs. 3.22 and 3.23 the magnetic field is plotted for a structure with air as the first

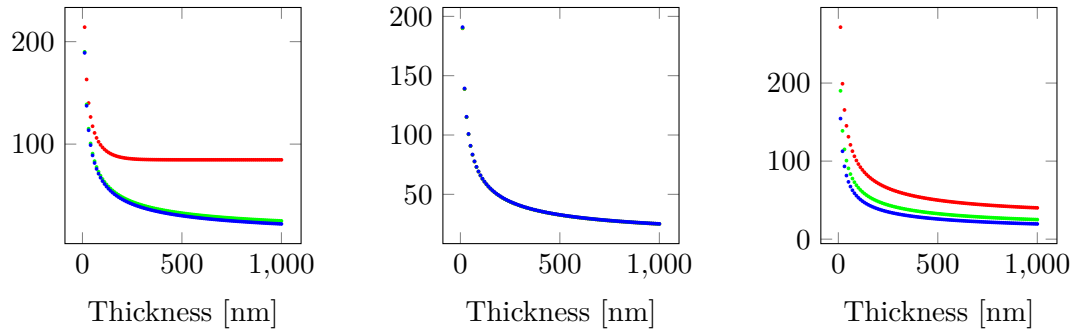

(a) *Varied wavelength. Red*=6×10^4 nm, *Green*=3×10^5 nm, *Blue*=6×10^5 nm.

(b) *Varied thickness of layer three. Red*=2 nm, *Green*=8 nm, *Blue*=32 nm.

(c) *Varied density of electrons in layer three. Red*=3.75×10^{12} cm^{-2}, *Green*=7.5×10^{12} cm^{-2}, *Blue*=1.125×10^{13} cm^{-2}.

Figure 3.14: *Real mode of a four layer structure as illustrated in fig. 3.1. The modes is calculated with varying thickness of layer two from* 1 nm *to* 1000 nm. *Layer one is a perfect conductor, layer two is AlGaN, layer three is GaN with additional free electrons, and layer four is neutral GaN. Unless otherwise noted the wavelength is* 3×10^5 nm *and layer three is* 8 nm *thick, and the electron density of layer three is* 7.5×10^{12} cm^{-2}.

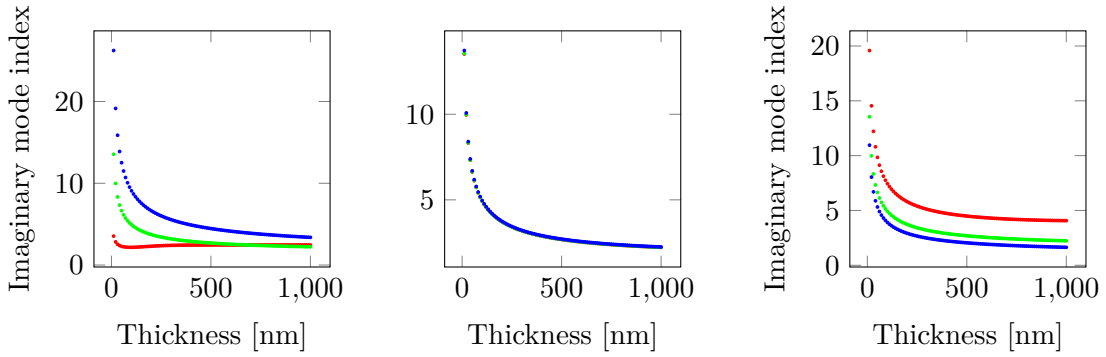

(a) *Varied wavelength. Red*=6×10^4 nm, *Green*=3×10^5 nm, *Blue*=6×10^5 nm.

(b) *Varied thickness of layer three. Red*=2 nm, *Green*=8 nm, *Blue*=32 nm.

(c) *Varied density of electrons in layer three. Red*=3.75×10^{12} cm^{-2}, *Green*=7.5×10^{12} cm^{-2}, *Blue*=1.125×10^{13} cm^{-2}.

Figure 3.15: *Imaginary mode of a four layer structure as illustrated in fig. 3.1. The modes is calculated with varying thickness of layer two from* 1 nm *to* 1000 nm. *Layer one is a perfect conductor, layer two is AlGaN, layer three is GaN with additional free electrons, and layer four is neutral GaN. Unless otherwise noted the wavelength is* 3×10^5 nm, *layer three is* 8 nm *thick, and the electron density of layer three is* 7.5×10^{12} cm^{-2}.

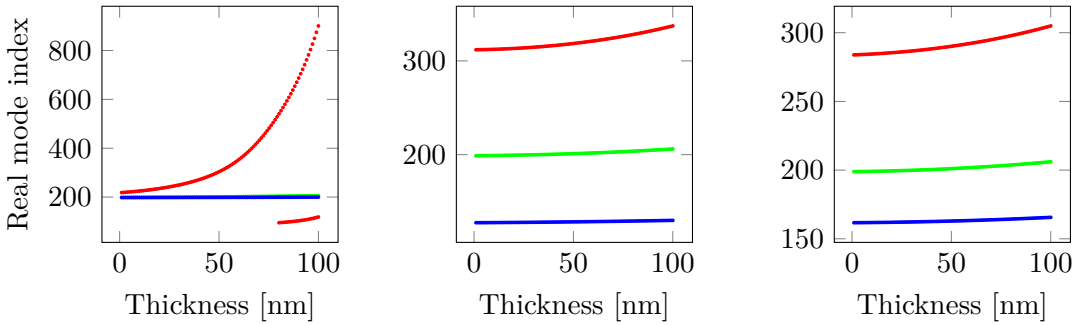

(a) *Varied wavelength.* *Red*=6×10^4 nm, *Green*=3×10^5 nm, *Blue*=6×10^5 nm.

(b) *Varied thickness of layer two.* *Red*=4 nm, *Green*=10 nm, *Blue*=25 nm.

(c) *Varied density of electrons in layer three.* *Red*=3.75×10^{12} cm^{-2}, *Green*=7.5×10^{12} cm^{-2}, *Blue*=1.125×10^{13} cm^{-2}.

Figure 3.16: *Real mode of a four layer structure as illustrated in fig. 3.1. The modes is calculated with varying thickness of layer three from* 1 nm *to* 100 nm. *Layer one is a perfect conductor, layer two is AlGaN, layer three is GaN with additional free electrons, and layer four is neutral GaN. Unless otherwise noted the wavelength is* 3×10^5 nm, *layer two is* 10 nm *thick, and the electron density of layer three is* 7.5×10^{12} cm^{-2}.

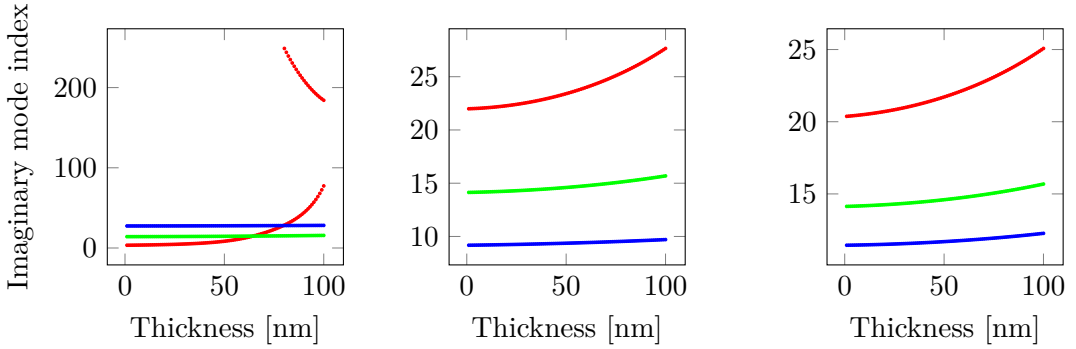

(a) *Varied wavelength.* *Red*=6×10^4 nm, *Green*=3×10^5 nm, *Blue*=6×10^5 nm.

(b) *Varied thickness of layer two.* *Red*=4 nm, *Green*=10 nm, *Blue*=25 nm.

(c) *Varied density of electrons in layer three.* *Red*=3.75×10^{12} cm^{-2}, *Green*=7.5×10^{12} cm^{-2}, *Blue*=1.125×10^{13} cm^{-2}.

Figure 3.17: *Imaginary mode of a four layer structure as illustrated in fig. 3.1. The modes is calculated with varying thickness of layer three from* 1 nm *to* 100 nm. *Layer one is a perfect conductor, layer two is AlGaN, layer three is GaN with additional free electrons, and layer four is neutral GaN. Unless otherwise noted the wavelength is* 3×10^5 nm, *layer two is* 10 nm *thick, and the electron density of layer three is* 7.5×10^{12} cm^{-2}.

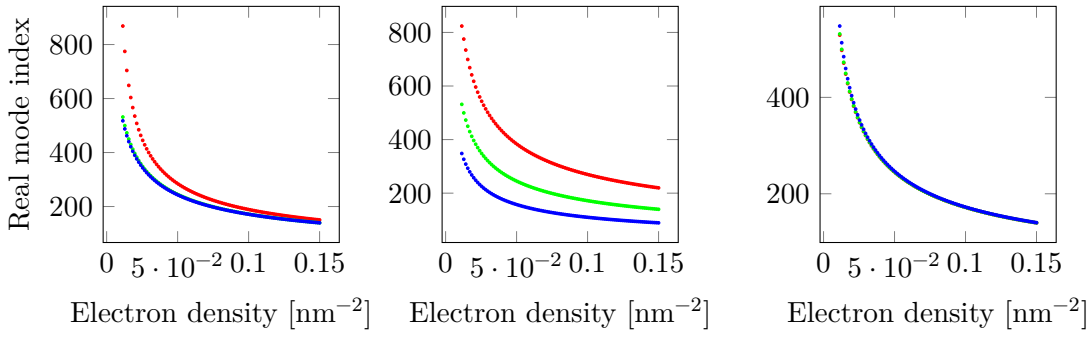

(a) *Varied wavelength.* *Red*=6×10^4 nm, *Green*=3×10^5 nm, *Blue*=6×10^5 nm.

(b) *Varied thickness of layer two.* *Red*=4 nm, *Green*=10 nm, *Blue*=25 nm.

(c) *Varied thickness of layer three.* *Red*=2 nm, *Green*=8 nm, *Blue*=32 nm.

Figure 3.18: *Real mode of a four layer structure as illustrated in fig. 3.1. The modes is calculated with varying electron densities in layer three from* 1×10^{12} cm^{-2} *to* 15×10^{12} cm^{-2}*. Layer one is a perfect conductor, layer two is AlGaN, layer three is GaN with additional free electrons, and layer four is neutral GaN. Unless otherwise noted the wavelength is* 3×10^5 nm*, layer two is* 10 nm *thick, and layer three is* 8 nm *thick.*

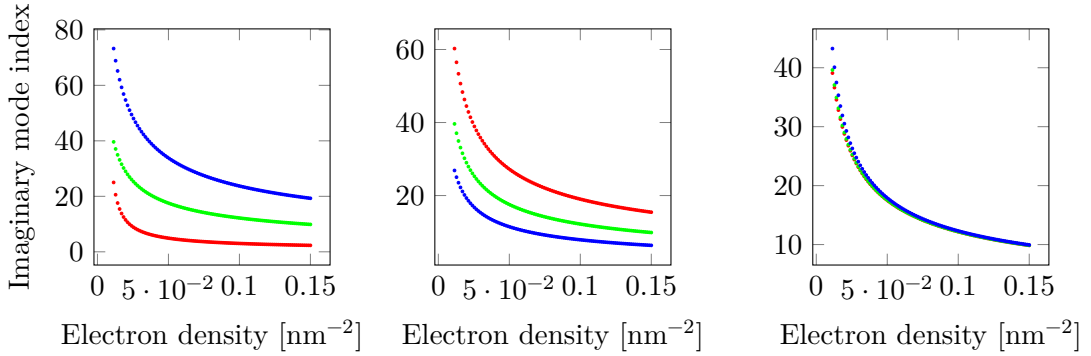

(a) *Varied wavelength.* *Red*=6×10^4 nm, *Green*=3×10^5 nm, *Blue*=6×10^5 nm.

(b) *Varied thickness of layer two.* *Red*=4 nm, *Green*=10 nm, *Blue*=25 nm.

(c) *Varied thickness of layer three.* *Red*=2 nm, *Green*=8 nm, *Blue*=32 nm.

Figure 3.19: *Imaginary mode of a four layer structure as illustrated in fig. 3.1. The modes is calculated with varying electron densities in layer three from* 1×10^{12} cm^{-2} *to* 15×10^{12} cm^{-2}*. Layer one is a perfect conductor, layer two is AlGaN, layer three is GaN with additional free electrons, and layer four is neutral GaN. Unless otherwise noted the wavelength is* 3×10^5 nm*, layer two is* 10 nm *thick, and layer three is* 8 nm *thick.*

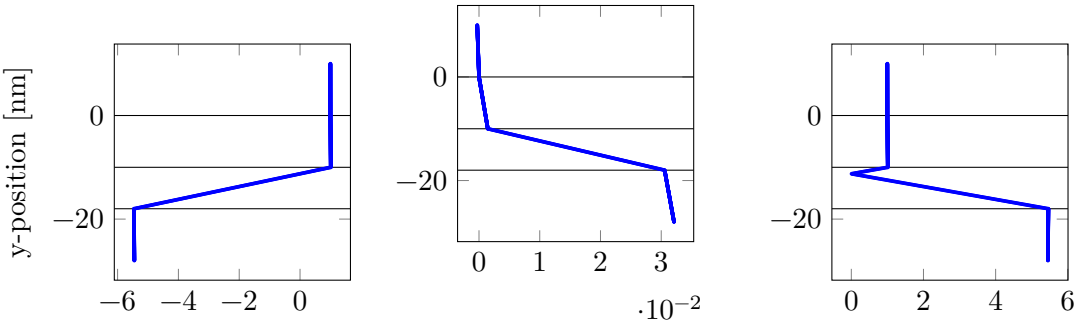

(a) *Real magnetic field.* **(b)** *Imaginary magnetic field.* **(c)** *Absolute magnitude of magnetic field.*

Figure 3.20: *Magnetic field at* $\lambda = 3.000\,000 \times 10^5$ nm *with a thickness of layer two of* 10 nm, *and layer three of* 8 nm, *and an electron density of* $7.500\,000 \times 10^{12}\,\mathrm{cm}^{-3}$, *where layer one is air. The mode found as a solution to* $f(k_x) = 0$ *eq. (3.11) is* $n_m = 1.027\,116 \times 10^1 + 1.376\,384i$. *The magnetic field is calculated* 10 nm *inside the two infinite layers one and four.*

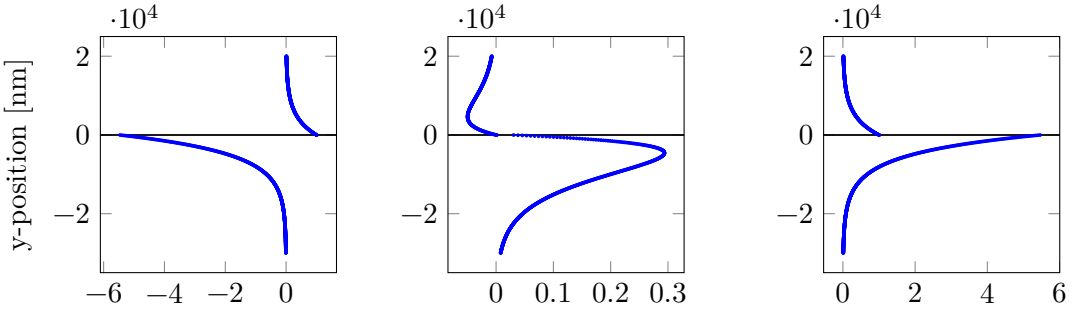

(a) *Real magnetic field.* **(b)** *Imaginary magnetic field.* **(c)** *Absolute magnitude of magnetic field.*

Figure 3.21: *Magnetic field at* $\lambda = 3.000\,000 \times 10^5$ nm *with a thickness of layer two of* 10 nm, *and layer three of* 8 nm, *and an electron density of* $7.500\,000 \times 10^{12}\,\mathrm{cm}^{-3}$, *where layer one is air. The mode found as a solution to* $f(k_x) = 0$ *eq. (3.11) is* $n_m = 1.027\,116 \times 10^1 + 1.376\,384i$. *The magnetic field is calculated in the y-range from* 20 000 nm *to* −30 000 nm.

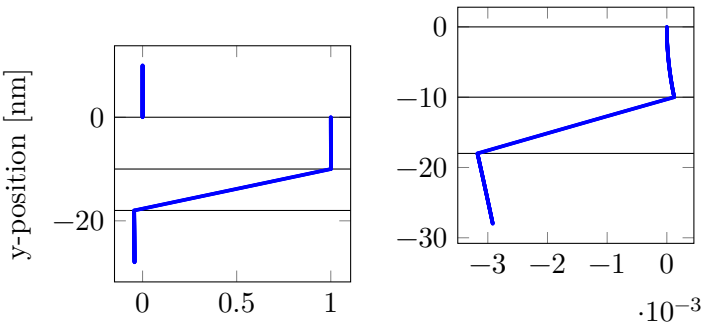

(a) *Real magnetic field.* **(b)** *Imaginary magnetic field.* **(c)** *Absolute magnitude of magnetic field.*

Figure 3.22: *Magnetic field at* $\lambda = 3.000\,000 \times 10^5$ nm *with a thickness of layer two of* 10 nm, *and layer three of* 8 nm, *and an electron density of* $7.500\,000 \times 10^{12}$ cm^{-3}, *where layer one is a perfect conductor. The mode found as a solution to* $f(k_x) = 0$ *eq. (3.11) is* $n_m = 1.990\,243 \times 10^2 + 1.416\,889 \times 10^1 i$. *The magnetic field is calculated* 10 nm *inside the two infinite layers one and four.*

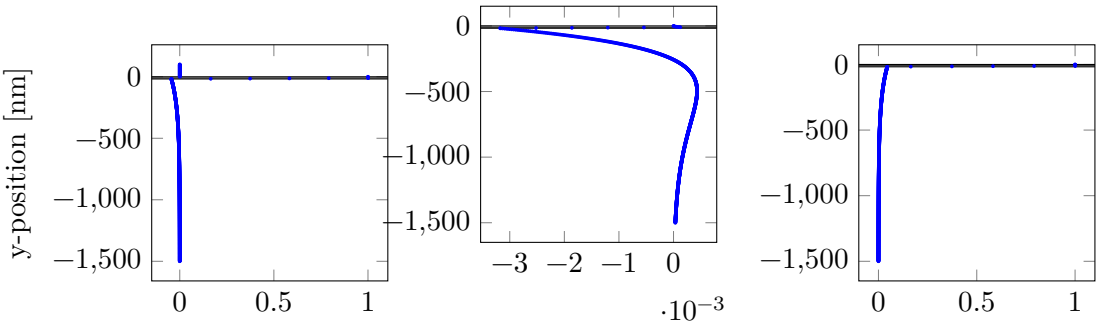

(a) *Real magnetic field.* **(b)** *Imaginary magnetic field.* **(c)** *Absolute magnitude of magnetic field.*

Figure 3.23: *Magnetic field at* $\lambda = 3.000\,000 \times 10^5$ nm *with a thickness of layer two of* 10 nm, *and layer three of* 8 nm, *and an electron density of* $7.500\,000 \times 10^{12}$ cm^{-3}, *where layer one is a perfect conductor. The mode found as a solution to* $f(k_x) = 0$ *eq. (3.11) is* $n_m = 1.990\,243 \times 10^2 + 1.416\,889 \times 10^1 i$. *The magnetic field is calculated in the y-range from* 100 nm *to* −1500 nm.

layer. The mode used in the calcualtions is $n_m = 1.990\,243 \times 10^2 + 1.416\,889 \times 10^1 i$.

4 Terahertz Response

This chapter is focused on using Green's function to calculate The magnetic field H and its normal derivative ϕ on the scatterer, the Poynting vector (amplitude), and the scattering cross section. The first section expands upon the calculations performed. The second section presents the calculated data.

4.1 Calculation

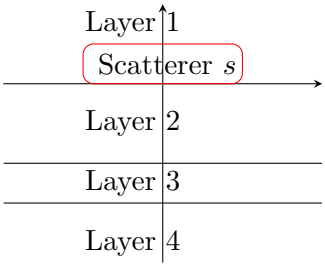

Figure 4.1: *Structure used for calculation of terahertz respones..*

Calculation of the response were performed in three steps. First the non-analytical part of the indirect Green's function is evaluated on a fixed grid at certain intervals. The result is then stored in a matrix, and saved for later. This calculation is performed for varying wavelengths, electron densities and thickness's of layers. Secondly eq. (2.84) is solved. Lastly the found filed H, and ϕ is used to calculate the response of the scatterer.

Figure 4.1 illustrates the structure for which the terahertz respones is calculated. Layer one is vacuum. Layer two is comprised of AlGaN. Layer three and four are both comprised of GaN. In layer three the electron density is increased. Calculation of the dielectric constant for this layer is describes in section 3.2.1. The scatterer is calculated as a very good conductor with a dielectric constant of $\epsilon_s = -10^10$. The distance along the scatterer t starts at the bottom of the left vertical section of scatterer, and goes clockwise along the scatter.

The standard values used for calculation if the response is

$$\begin{aligned} \lambda &= 300\,000\,\mathrm{nm}\,, \\ \text{Electrondensity} &= 7.5 \times 10^{12}\,\mathrm{cm}^{-2}\,, \\ d_2 &= 10\,\mathrm{nm}\,, \\ d_3 &= 8\,\mathrm{nm}\,, \\ \Delta_j &= 1\,\mathrm{nm} \end{aligned}$$

and the scatterer is 10 nm high, 704 nm wide. The rounded corners are 3 nm in radius.

The size of the indirect matrix is decided by two factors. The dimensions and position of the scatterer, and by the desired resolution. Here the scatterer rest on layer 2, with the bottom at $z = 0$, giving a possible range of $0 \leq z + z' \leq 2h$, where h is the heigh of the scatterer. The centre of the scatterer is placed at $x = 0$, though this does not influence the range of $-w \leq x - x' \leq w$ where w is the width of the scatterer. The range $0 \leq x - x' \leq w$ should work fine since the indirect function is symmetrical around the x-axis. Experimentation revealed that a resolution of 1 nm to 2 nm yield nearly identical matrices. With this result it was chosen to use a resolution of 2 nm for the calculations. After choosing the values for which the indirect matrix will be calculated, Matlab was used to perform the numerical evaluation of the integral

$$g^{(i)} = \frac{i}{2\pi} \int_0^\infty \frac{\cos(k_x|x - x'|\left(r(k_x) - \frac{\epsilon_2 - \epsilon_1}{\epsilon_2 + \epsilon_1}\right) \mathrm{e}^{\mathrm{i}k_{y,1}(y+y')})}{k_{y,1}} \,\mathrm{d}k_x \,, \tag{4.1}$$

and its derivatives with respect to x' and y'

$$\frac{\partial g^{(i)}}{\partial x'} = \frac{i}{2\pi} \int_0^\infty \frac{k_x \sin(k_x|x - x'|\left(r(k_x) - \frac{\epsilon_2 - \epsilon_1}{\epsilon_2 + \epsilon_1}\right) \mathrm{e}^{\mathrm{i}k_{y,1}(y+y')})}{k_{y,1}} \,\mathrm{d}k_x \,, \tag{4.2}$$

$$\frac{\partial g^{(i)}}{\partial y'} = \frac{i}{2\pi} \int_0^\infty \cos(k_x|x - x'|\left(r(k_x) - \frac{\epsilon_2 - \epsilon_1}{\epsilon_2 + \epsilon_1}\right) \mathrm{i}\,\mathrm{e}^{\mathrm{i}k_{y,1}(y+y')}) \,\mathrm{d}k_x \,. \tag{4.3}$$

The initial range from $k_x = 0$ to $k_x = 6k_0$ were solved with an ellipse into the complex plane. When $z + z' = 0$ Matlab's inbuilt integral solver were unable to solve the integral most of the time, this was circumvented by setting the value of $z + z' = 1 \times 10^{-5}$ instead.

The first step in generating the elements for eq. (2.84) is to discretise the surface of the scatterer. First a desired length of each segment is chosen, this is then used to find the number of segments in the corners and their actual length. With this length the number of segments along the horizontal and vertical segments is calculated, trying to maintain the smallest deviation in lengths. Then the postion and normal vectors for each segment was found. Calculating the elements in $\overline{\overline{A}}$, $\overline{\overline{B}}$ is for the most part trivial, though both sets of equations contain singularities. When $i \neq j$ it can be done by calculating eqs. (2.63) and (2.71) and multiplying the result with the segment length Δ_j directly. While keeping in mind that $g_s^{(i)} = 0$ The integral part of eq. (2.71) is found by interpolating in the indirect Green's matrix calculated earlier.

Having solved the eq. (2.84) for $\overline{H}$ and $\overline{\phi_1}$, the found values can be used with eqs. (2.61) and (2.62) to calculate the scattered far field, which in turn can be used to calculate the magnitude of the poynting vector eq. (2.28) and scattering cross section eq. (2.31).

4.2 Result

The first calculations performed was to determine the optimal length of the scatterer with the given standard values given in section 4.1. In section 3.2.3 it was found that the

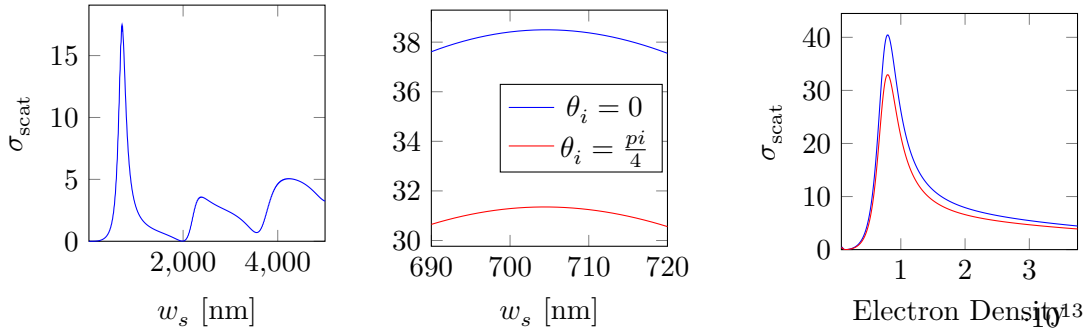

(a) *Scattering cross section as a function of width* 10 nm *to* 5000 nm. *Each segment in the discretise scatterer is* 4 nm *wide.*

(b) *Scattering cross section as a function of width* 690 nm *to* 720 nm. θ_i *is the incident angle for the radiation. Each segment in the discretise scatterer is* 1 nm *wide.*

(c) *Scattering cross section as a function of electron density* $7.5 \times 10^{11}\,\mathrm{m}^{-3}$ *to* $3.75 \times 10^{13}\,\mathrm{m}^{-3}$. θ_i *is the incident angle for the radiation.*

Figure 4.2: *Scattering cross section as a function of the width of the scatterer* w_s*, or electron density. The calculation is otherwise performed with standard values as given in section 4.1.*

used values results in a guided mode with $n_m \approx 200$. With this value the width of the scatterer were approximated to

$$w_s = \frac{\lambda}{2n_m} \approx 750\,\mathrm{nm}\,. \tag{4.4}$$

The position of the peak in fig. 4.2a is used at the basis for the calculation of fig. 4.2b. From fig. 4.2b the optimal width is found to be approximatly 704 nm. Figure 4.2a is calculated up to 5000 nm. To achieve this the resolution of discretisation on the scatter was reduced to avoid using excessive time on the computations. Comparing this with fig. 4.2b it is clear that this compromise has changed the amplitude of the result drastically, though the position of the peak are similar. In figs. 4.2b and 4.2c the scattering cross section is calculated for radiation with a incident angle of $\theta = 0$ and $\theta = \frac{\pi}{4}$ as expected the suboptimal incident angle reduced scattering cross section, while retaining its form.

Figure 4.2c shows a clear peak at around the expected electron density of $7.5 \times 10^{12}\,\mathrm{cm}^{-2}$. At lower electron densities the scattering cross section reduces to 0. While increasing the electron density reduces the scattering cross section, it seem to level of at about one tenth of its peak value.

Figure 4.3 show the result of the calculations with varying heights. For all of the figures it seem that the incident angle does not influence the response of the scatterer beyond reducing the amplitude. It seem that using suboptimal incident angles results in a constant factor difference. Figure 4.3a has a clearly defined peak at 9.5 nm This is a bit lower than the expected 10 nm. Figure 4.3b shows that the height of layer three only has a small influence on the optical response. Figure 4.3c Indicates that the optical cross section is highly influenced by the height of the scatterer.

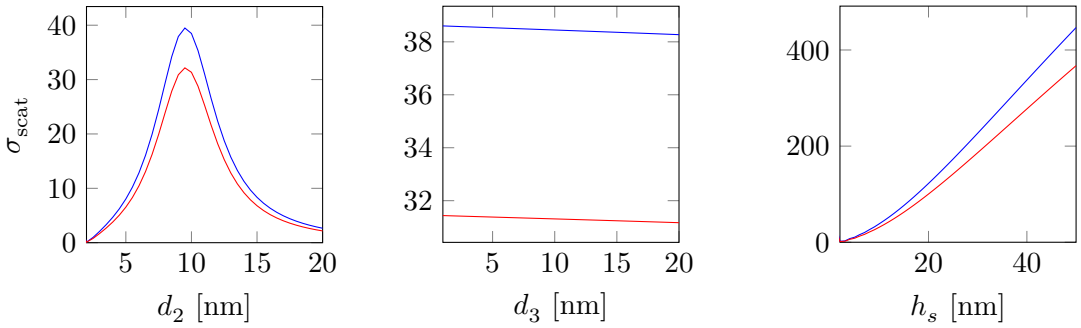

(a) *Scattering cross section as a function of height of layer 2 d_2 2 nm to 20 nm..*

(b) *Scattering cross section as a function of height of layer 3 d_3 1 nm to 20 nm..*

(c) *Scattering cross section as a function of height of scatterer h_s 2 nm to 20 nm..*

Figure 4.3: *Scattering cross section as function of the height of Layer 2, layer 3, and the scatterer respectively. θ_i is the incident angle for the radiation. The calculation is otherwise performed with standard values as given in section 4.1.*

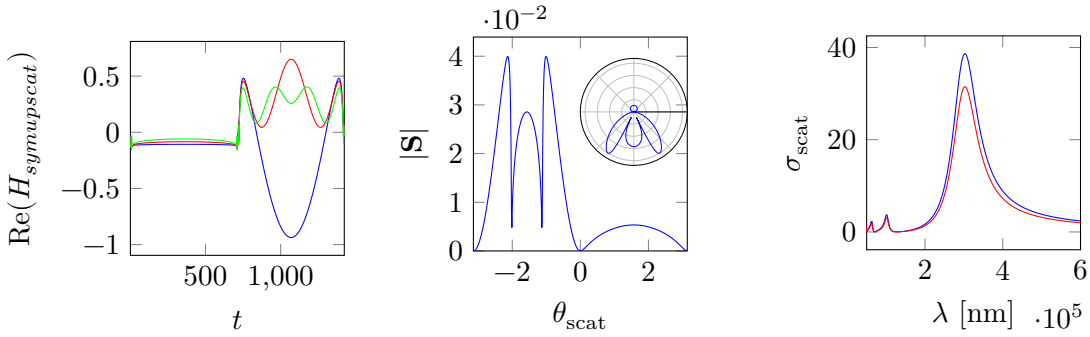

(a) *Magnetic field on scatterer calculated at different wavelengths. t is the distance along the scatterer. Blue is $\lambda_i = 302\,000$ nm, Red $\lambda_i = 102\,000$ nm, and Green $\lambda_i = 64\,000$ nm.*

(b) *Magnitude of the scattered far fields Poynting vector. Insert in upper right corner is a polar plot of the same data.*

(c) *Scattering cross section as a function of wavelength λ 50 000 nm to 600 000 nm. Blue is $\theta_i = 0$, Red $\theta_i = \frac{\pi}{4}$.*

Figure 4.4: *Unles otherwise noted the calculation is performed with standard values as given in section 4.1.*

Figure 4.4c shows that the scattering is most prominent at the resonance frequency, it also show a third, and a fifth harmonic. As with the other calculated at suboptimal incident angles the difference in amplitude seem to be a constant factor. The Poynting vector shown in fig. 4.4b shows that a small part of the radiation is reflected upwards. Most of the transmitted radiation is focused in a centre cone and two ”wings”. The wings appear as a result of the scattered radiation nearing the critical angle of the interface. The real part of the magnetic field shown in fig. 4.4a for three different wavelength corresponds to the three peaks in fig. 4.4. BLue to the rightmost peak, red to the centre peak, and green to the leftmost peak. The first half of the graph corresponds roughly to top of the scatterer, and the second half to the bottom. As expected the graph at the resonance frequency is a half wave, at the third harmonic it is a three and a half wave, and the fifth harmonic is a five and a half wave.

5 Conclusion

From the data I can se that the thickness of layer 3 (the semiconducting layer) only has a minor influence over the renascence og the media. Since the electron density of this layer is easiest to control by applying a static current to the scatterer dragging electrons from layer 4, the thickness of layer 3 is dynamic. This makes this a desirable observation.

From the data it is evident that it is possible to tune the frequency response of the structure, by changing the electron density, the thickness of layer 2, and the width of the scatterer. Response to varying the height of the scatterer puzzles me. While I expect some response from changing the height I did not expect it to dominate so clearly.

As noted in chapter 4 the predicted width of the scatterer from chapter 3 is about 50 nm larger than the one found in chapter 4. This might be caused by the difference in dielectric constant for the scatterer compared to the perfect conductor used in chapter 3. Experimenting with changing the dielectric constant seem to support this hypothesis, but since making the conductor better than it currently is results in Matlab warning me about potential singular matrices, this can not currently be verified by me.

Another explanation could be that the data is not fully converged. While this by first glance would be easy to confirm, it is not. Increasing the resolution on the scatterer increases the memory usage, and the calculations already places a huge demand on memory. I tried with to test for convergence with a less wide scatter. This showed that while not fully converged, it did not change much by increasing the resolution. A curious observation I made while testing for convergence, was that the result seemed to oscillate. While increasing the density of segments the cross section decreases linearly until it jumps up. This repeats with increasing distance between each jump. While the first few jumps decreased in size, the following jumps were of about the same size.

As it is implemented in this thesis i would not recommend using Green's function for calculation of terahertz response of a semiconducting structure.

The next step would be to abandon the assumption that the magnetic field is constant along each segment. Alternatively the discretisation of the scatterer could be changed, so that density of segments where the magnetic field varies most rapidly is increase, while decreasing the density elsewhere.

References

[1] G. P. Gallerano et al. 'Overview of terahertz radiation sources.' In: (Jan. 2004). URL: https://accelconf.web.cern.ch/AccelConf/f04/papers/FRBIS02/FRBIS02.PDF.

[2] Megan Leahy-Hoppa, Michael Fitch and Robert Osiander. 'Terahertz spectroscopy techniques for explosives detection'. eng. In: *Analytical and Bioanalytical Chemistry* 395.2 (2009-09), pp. 247, 257. ISSN: 1618-2642.

[3] K Ishigaki et al. 'Direct intensity modulation and wireless data transmission characteristics of terahertz-oscillating resonant tunnelling diodes'. eng. In: *Electronics Letters* 48.10 (2012-05-10), pp. 1, 2. ISSN: 00135194. URL: http://search.proquest.com/docview/1616437295/.

[4] A J Fitzgerald. 'An introduction to medical imaging with coherent terahertz frequency radiation'. eng. In: *Physics in Medicine and Biology* 47.7 (2002-04-07), R67, R84. ISSN: 0031-9155. DOI: 10.1088/0031-9155/47/7/201.

[5] B.S Alexandrov et al. 'DNA breathing dynamics in the presence of a terahertz field'. eng. In: *Physics Letters A* 374.10 (2010), pp. 1214, 1217. ISSN: 0375-9601. DOI: 10.1016/j.physleta.2009.12.077.

[6] Eric S. Swanson. 'Modeling DNA response to terahertz radiation'. In: *Phys. Rev. E* 83 (4 Apr. 2011), p. 040901. DOI: 10.1103/PhysRevE.83.040901. URL: https://link.aps.org/doi/10.1103/PhysRevE.83.040901.

[7] Thomas M. Søndergaard. *Green's Function Integral Equation Methods in Nano-Optics*. English. First. CRC Press, 2019. ISBN: 978-0-8153-6596-9. DOI: 10.1201/9781351260206.

[8] David J. Griggiths. *Introduction to Electrodynamics*. English. Fourth. Pearson, 2014. ISBN: 978-1-29202-142-3.

[9] Eugene Hecht. *Optics*. English. Fifth. Pearson, 2017. ISBN: 978-1-292-09693-3.

[10] Eugene Hecht. *Advanced Engineering Mathematics*. English. Tenth. Wiley, 2011. ISBN: 978-0-470-64613-7. URL: www.wiley.com/go/global/kreyszig.

[11] Murray R. Spiegel, Seymour Lipschutz and John Liu. *Mathematical Handbook of Formulas and Tables*. English. Fourth. McGraw-Hill, 2013. ISBN: 978-0-07-179537-1.

[12] A. V. Muravjov et al. 'Temperature dependence of plasmonic terahertz absorption in grating-gate gallium-nitride transistor structures'. In: *Applied Physics Letters* 96.4 (2010), p. 042105. DOI: 10.1063/1.3292019.